

## Resilience Patterns of Multiscale Human Mobility Under Extreme Rainfall Events Using Massive Individual Trajectory Data

Yao Yao, Lin Liang, Yatao Zhang, Yujia Wang, Zhihui Hu, Yunpeng Fan, Qingfeng Guan, Renhe Jiang & Ryosuke Shibasaki

To cite this article: Yao Yao, Lin Liang, Yatao Zhang, Yujia Wang, Zhihui Hu, Yunpeng Fan, Qingfeng Guan, Renhe Jiang & Ryosuke Shibasaki (02 Jan 2025): Resilience Patterns of Multiscale Human Mobility Under Extreme Rainfall Events Using Massive Individual Trajectory Data, *Annals of the American Association of Geographers*, DOI: [10.1080/24694452.2024.2435927](https://doi.org/10.1080/24694452.2024.2435927)

To link to this article: <https://doi.org/10.1080/24694452.2024.2435927>



© 2024 The Author(s). Published with license by Taylor & Francis Group, LLC.



Published online: 02 Jan 2025.



Submit your article to this journal [↗](#)



View related articles [↗](#)



View Crossmark data [↗](#)

# Resilience Patterns of Multiscale Human Mobility Under Extreme Rainfall Events Using Massive Individual Trajectory Data

Yao Yao,<sup>a,b</sup>  Lin Liang,<sup>a</sup> Yatao Zhang,<sup>c</sup>  Yujia Wang,<sup>a</sup> Zhihui Hu,<sup>a</sup> Yunpeng Fan,<sup>a</sup> Qingfeng Guan,<sup>a</sup>  Renhe Jiang,<sup>b</sup> and Ryosuke Shibasaki<sup>d</sup>

<sup>a</sup>School of Geography and Information Engineering, China University of Geosciences, China; <sup>b</sup>Center for Spatial Information Science, The University of Tokyo, Japan; <sup>c</sup>Future Resilient Systems, Singapore-ETH Centre, ETH Zurich, Singapore; <sup>d</sup>Interfaculty Initiative in Information Studies & Graduate School of Interdisciplinary Information Studies, The University of Tokyo, Japan

Understanding human mobility's resilience during extreme rainfall is paramount for enhancing disaster response and urban resilience. Most studies, however, have overlooked the complexity of resilience patterns across scales, missing out on the varied spatial anomalies and their underlying causes. To bridge this gap, we propose a framework using massive individual trajectory data to dissect resilience patterns of human mobility across scales. By leveraging a dynamic network model, we quantify human mobility flows and employ resilience curves to determine resilience patterns at urban-agglomeration and regional scales. Our study, centering on the extreme rainfall from Typhoon Mawar, covers Osaka and Nagoya in Japan. The findings reveal a marked reduction in human movement, although the structure of mobility networks remains relatively unchanged. Based on the quadrant distribution of inflows and outflows, we reveal that the ratio of abnormal to normal resilience patterns in human mobility stands at approximately 3:2, a consistency maintained across both scales. Interestingly, abnormal resilience patterns are intricately linked to local geographical settings of the built environment, revealing disparities based on income, gender, and age. These insights are invaluable for policymakers to improve postdisaster recovery efforts and guide future urban infrastructure development toward greater resilience. *Key Words: extreme rainfall, human mobility, resilience patterns, trajectory data, urban agglomeration.*


The Intergovernmental Panel on Climate Change (IPCC) Sixth Assessment Report highlights a significant uptick in extreme weather events, including heavy rainfall, hurricanes, and floods, since the 1970s (Scott et al. 2024). This escalation is attributed to the synergistic effects of climate change, a burgeoning global population, and rapid urban development (Reichstein, Riede, and Frank 2021; Mehrabi et al. 2022). Extreme climate disasters have become a constant risk, causing direct asset losses averaging over \$300 billion annually (Hallegatte et al. 2016; Smiley et al. 2022). The most significant proportion of natural disasters consists of floods caused by extreme rainstorms, resulting in substantial economic losses and severe socio-economic development impacts (Hino and Nance 2021;

Rentschler, Salhab, and Jafino 2022). Under circumstances of rapid global urbanization, the development of city clusters has become an essential model for future urban development. The sustainable and safe development of urban clusters is a matter of national future and destiny (Fang, Wang, and Ma 2018; United Nations 2018). Therefore, it is crucial to understand the resilience of urban agglomeration systems amid extreme rain and flood disasters, which can provide references for reducing the economic losses caused by climate change and supporting the pursuit of sustainable development goals (SDGs).

Resilient cities emphasize the capacity of complex urban systems to absorb external disruptions and either restore their original state or reach a new equilibrium through processes of learning and

## ARTICLE HISTORY

Initial submission, February 2024; revised submissions, June and September 2024; final acceptance, October 2024

CORRESPONDING AUTHOR Yatao Zhang  yatzhang@ethz.ch

© 2024 The Author(s). Published with license by Taylor & Francis Group, LLC.

This is an Open Access article distributed under the terms of the Creative Commons Attribution License (<http://creativecommons.org/licenses/by/4.0/>), which permits unrestricted use, distribution, and reproduction in any medium, provided the original work is properly cited. The terms on which this article has been published allow the posting of the Accepted Manuscript in a repository by the author(s) or with their consent.

reorganization (Cutter et al. 2008; Kontokosta and Malik 2018). External perturbations usually refer to acute shocks and chronic stresses, such as natural disasters, climate change, environmental pollution, and public health emergencies (Y. Zhang et al. 2024). Taking climate disasters as an example, they include heavy rainstorms, hurricanes, droughts, and floods. In flood risk research, the concept describes the capacity to effectively withstand flooding impacts and rapidly restore essential functions to minimize losses (Liao 2012; Pimm et al. 2019). In recent years, the concept of resilience has been increasingly integrated into urban planning and urban disaster management. So far, several methods have been proposed to measure urban resilience, including qualitative and quantitative approaches (Rus, Kilar, and Koren 2018). Qualitative measures explore the components of resilience through empirical research and structured interviews. Quantitative assessments encompass statistical analyses and validation of factors influencing resilience and numerical measures of resilience levels (RLs; Sharifi and Yamagata 2016; Tong 2021). Existing studies typically employ classical time-series performance curves from quantitative assessment methods to characterize the system response during preevent, midevent, and postevent phases. This approach has become the cornerstone of resilience-related urban studies because its concepts have been associated quite closely with reliability, flexibility, stability, and robustness (Cimellaro, Reinhorn, and Bruneau 2010; Poulin and Kane 2021; Perera and Hong 2023).

Moreover, extensive human activities within cities imbue urban systems with heightened complexity and dynamism, rendering them particularly susceptible and variable in response to external shocks (Batty 2013; Kraemer et al. 2020). This phenomenon is especially evident in extreme climate disasters, where the intricate interplay of human mobility and urban spaces challenges the resilience capacities of cities (Ronco et al. 2023). In this situation, accurately assessing human mobility patterns, both spatially and temporally, emerges as a pivotal factor in providing novel insights essential for a wide range of urban planning, such as traffic prediction, resource distribution, public health monitoring, and disaster management (Santana et al. 2023; Yao et al. 2023). Furthermore, there has been a limited integration of human mobility data in measuring urban resilience. Previous empirical studies have encountered significant challenges

due to data constraints and the lack of effective resilience indicators (Kontokosta and Malik 2018; Barrett et al. 2021). The complexity of accounting for spatio-temporal dynamics in how human mobility adapts to and recovers from events like extreme rainfall further complicates the development of effective and robust measures of resilience.

Existing studies indicate that changes in human mobility during extreme disaster situations often adhere to the conventional bathtub-shaped resilience curve (Panteli et al. 2017; Hossain et al. 2021). Nevertheless, the majority of these studies are quantitative analyses that focus primarily on the adaptability and resilience of urban systems (i.e., the RL) when confronted with external pressures (Tang et al. 2023), but neglect to explore further diverse patterns of spatial abnormal resilience. Consequently, they fall short of accurately portraying the multifaceted responses of urban systems to diverse pressures and challenges, leading to an information gap that hampers the development of planning strategies addressing these unique resilience patterns. A recent study underscored significant socioeconomic and racial disparities in resilience and evacuation patterns of urban populations during hurricane disaster (Hong et al. 2021). Therefore, scrutinizing these disparities is crucial for a more comprehensive understanding of collective responses to urban hazards across different zoning scales, which can contribute to enhancing a city's capacity to resist extreme disasters, expedite recovery, and minimize damages.

Current research exhibits a gap in understanding multiscale resilience, which refers to the capacity of systems to withstand and recover from adverse events across different levels, such as country, city, community, and individuals (Tong 2021). Theoretical frameworks for multiscale urban resilience are still underdeveloped, and this lack of multiscale knowledge further hinders the development of integrated assessment models. In addition, existing data sets basically focus on specific scales without integrating data across multiple levels, posing challenges in analyzing resilience variations across scales. To enhance urban resilience to climate hazards, constructing multiscale assessments has become imperative.

With the emergence of massive spatiotemporal big data, research on urban resilience based on human mobility data has become a hot topic (Sarker et al. 2020). Trajectory data is a type of sequence data with spatial and temporal characteristics that

can be used to simulate human behaviors in response to natural disasters. These data can be harnessed to build more potent and effective models of urban dynamics, thereby elucidating the unique dynamics and complexities inherent to urban environments (Duan et al. 2023). Furthermore, they provide empirical support to explore the evolution of urban population dynamics and quantify urban resilience in the context of natural disasters (Kryvasheyev et al. 2016). This study leverages extensive individual trajectory data to develop a framework that assesses urban mobility resilience across different scales in response to extreme rainstorms. By analyzing human mobility responses to disasters and the causes of their impacts, our research is critical in guiding future urban spatial planning for more sustainable and equitable long-term urban development.

This study addresses two critical questions: (1) What insights can large-scale trajectory data provide into multiscale human mobility during extreme rainstorms, including the processes of impact and recovery? (2) How can diverse resilience patterns in human mobility be further explored and their underlying causes explained? This study focuses on the rainstorm triggered by Typhoon Mawar in Japan, aiming to dissect human mobility resilience across scales under rainstorm disasters. We quantify the human mobility RL and reveal the resilience response pattern of human mobility behavior to disasters. Subsequently, this research aims to uncover the associative mechanisms between resilience patterns and sociodemographic factors, providing targeted recommendations for policymakers.

In addition, our contributions are threefold. (1) We propose an evaluation framework to assess the resilience of human mobility across multiple scales during rainstorm disasters. Using large-scale trajectory data, we quantify the level of resilience within human mobility and analyze the dynamic characteristics of the human mobility network structure. (2) We uncover distinct human mobility resilience patterns across various scales. We find that the ratio of abnormal to normal resilience patterns in human activities is approximately 3:2, and this proportion remains consistent at both scales. (3) We explore the relationship between the resilience of human mobility and sociodemographic factors. Our findings indicate that exceptional resilience patterns are closely related to the geographical and built environment context, with noticeable variations across income levels, genders, and age groups.

## Literature Review

The concept of resilience, first introduced by Holling (1973) to describe an ecosystem's capacity to return to equilibrium after external disturbances, has since evolved into a central framework for urban disaster prevention (Rus, Kilar, and Koren 2018). This framework has gained considerable attention, providing a basis for urban development aimed at adapting to environmental changes and mitigating the impacts of natural disasters. Recent studies have increasingly focused on methodologies to assess and enhance the ability of urban systems to withstand and recover from such events.

When assessing urban resilience, both model-based and metric-based methods are commonly employed to evaluate system performance (Y. Zhang et al. 2024). Model-based approaches typically involve scenario-based techniques and system configuration modeling to estimate system evolution and its emergent properties (Linkov et al. 2020). For instance, Li et al. (2022) developed a resilience assessment model that integrates environmental, socioeconomic, and management-based indicators to evaluate the resilience of Kunshan City to flooding disasters. These methods are particularly effective for long-term resilience forecasting and strategic planning of complex systems. They often struggle, however, to capture the immediate changes and short-term fluctuations that occur in urban systems during disaster events.

In contrast, metric-based methods, which are the focus of this study, involve the assessment of key information metrics related to various system attributes. Among these methods, the resilience curve illustrates a system's capacity to absorb external shocks, recover, and reach a new equilibrium, depicting its dynamic performance under specific scenarios (Perera and Hong 2023). For example, Y. Zhang et al. (2024) combined nighttime light data with resilience curves to develop an evolving urban resilience index that measures global urban resilience and examines the influence of socioeconomic factors. Similarly, Hong et al. (2021) employed indicators like impact magnitude and recovery time within resilience curves to dynamically represent city's response to disasters, facilitating the development of targeted interventions. Overall, metric-based methods offer a more intuitive and responsive framework for capturing real-time system performance, making them particularly effective in dynamically tracking the immediate impacts of disasters and the system's adaptive responses across varying scenarios.

When exploring urban resilience in response to natural hazards, massive individual trajectory data have proven effective for representing resilience metrics and modeling human dynamics within resilience curves (Duan et al. 2023). This study aims to investigate the impacts of extreme rainfall events on urban human mobility, offering new insights into behavioral responses to disasters. In this case, examining human responses before, during, and after such events is crucial for understanding urban resilience and the system's recovery process (Santana et al. 2023), making metric-based methods well-suited for modeling and evaluating the performance of urban systems. Therefore, this study develops a comprehensive urban resilience assessment framework by using individual trajectory data and resilience curves. This approach allows us to quantify human mobility resilience and conduct dynamic assessments of system recovery, effectively capturing resilience patterns at various scales during extreme rainfall events.

## Study Area and Data

The study area is the Osaka and Nagoya metropolitan areas in Japan, as shown in Figure 1. For our study, we used boundary vector data sourced from

the Global Administrative Divisions Database (GADM), renowned for its detailed spatial data on administrative boundaries. The Osaka and Nagoya metropolitan areas are located along the Pacific coast of Honshu Island. This region is frequently affected by typhoons and heavy rainfall, making it a high-incidence area for extreme weather events. In addition, the study area is densely populated and economically advanced and is a core component of Japan's Pacific Coast urban agglomeration. These geographic, climatic, and economic characteristics are representative of coastal regions, highlighting the challenges faced by Japan and other coastal cities in coping with extreme rainfall.

On 1 June 2023, Typhoon Mawar instigated a prolonged period of substantial rainfall along Japan's southern coastline, triggering landslides, mudslides, and floods. By 2 p.m. on 3 June 2023, the Japan Meteorological Agency (JMA) declared that Typhoon Mawar had transitioned into a temperate cyclone. The large-scale mobile trajectory data employed in this study were provided by the Research Center for Spatial Information Science (CSIS) of the University of Tokyo. The data span eleven days from 28 May 2023 to 8 June 2023, covering the entire period of Typhoon Mawar's impact on Japan. It consists of 35,148,932

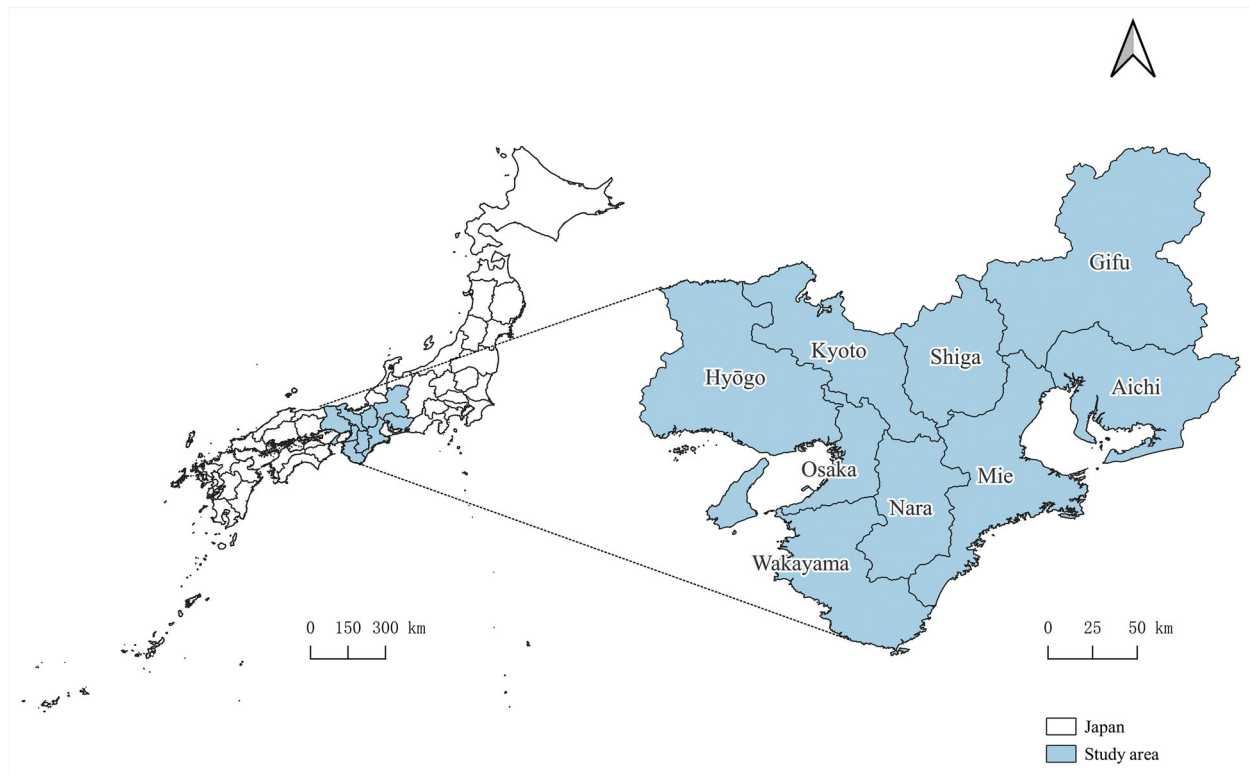


**Figure 1.** Study area: the Osaka and Nagoya metropolitan areas in Japan. The vector map data for the study area was obtained from the Global Administrative Divisions Database (<https://gadm.org/>).



high-fidelity geospatial records, including user IDs, timestamps, latitude, longitude, and so on, sourced from users' mobile devices within the study area. In this study, we aggregated the users' mobile records to the 1 km  $\times$  1 km grid and generated the origin–destination (OD) records.

In this study, we use point-of-interest (POI) data to explore the spatial distribution of resilience patterns. POI data have been proven effective in characterizing the socioeconomic and functional structure of cities (Yao et al. 2017). The POI data used were supplied by the University of Tokyo's CSIS under the auspices of the No. 1263 Joint Research Program in collaboration with ZENRIN Co., Ltd. To analyze the relationship between resilience patterns and urban functions, we selected POI data from eight distinct categories: tourism and sightseeing, transportation and logistics, recreation and entertainment, hotel and accommodation, food and beverage, commerce, education, and construction. Subsequently, we calculated the density of each POI category by enumerating the data points within each 1 km  $\times$  1 km grid.

In addition, we obtained the precipitation data and early warning systems from the JMA (see <https://www.jma.go.jp/>). We also sourced the population data, male-to-female sex ratio, population ratio by age, and Japan Community Survey (household economy, insured data) from the Statistical Bureau of the Ministry of Internal Affairs and Communications of Japan (see <https://www.stat.go.jp/>). Also, we used the Digital Elevation Model (DEM) data from the General Bathymetric Chart of the Oceans (see <https://www.gebco.net/>).

## Method

This study proposes a multiscale resilience computing framework on human mobility using trajectory data under extreme rainfall events. The framework adopts a dynamic network model to quantify human mobility and calculates the RL at the urban agglomeration scale through the conceptual resilience curve. Then, we define quadrant charts to analyze the radio and spatial distribution of the resilience patterns. These patterns are further analyzed and validated within the subnetwork clusters at the regional scale. We also calculate the RL at the regional scale through the conceptual resilience curve. Finally, the study employs correlation analysis and bivariate Moran's  $I$  analysis to elucidate

the relationship between abnormal resilience patterns, RLs, and social factors. The details of this proposed framework are shown in Figure 2.

### Quantifying Changes in Human Mobility and Resilience Level

Given an extreme rainfall event, this study develops the entire narrative by designating an eleven-day observation window for resilience analysis, as this duration adequately encompasses the entire events from the occurrence of the disaster, its impact on human mobility, to the eventual return to normal conditions. The selected time observation window has been proven to capture the entire cycle of human mobility pattern changes, thereby allowing for a comprehensive assessment of the event's impact (F. Zhang et al. 2019). The period of peak rainfall is defined as the during-event phase, with the four preceding days as the preevent phase and the four following days as the postevent phase. By discretizing the study area into 1 km  $\times$  1 km grids, we construct the mobility network by using the OD flux of human mobility data in the preevent, during-event, and postevent phases. This network features the origin and destination of the spatiotemporal movements as nodes and the trips as edges.

The network average degree and total edge weight are important attributes that reflect the structural features of networks (Yuan et al. 2018). The degree of a mobility network node represents the number of edges or connections the node has with other nodes in the network. The total edge weight (i.e., average daily OD flux) represents the average daily flow across all edges in the network, which is positively correlated with the flow intensity in the mobility network. In this study, it represents the overall human mobility on a daily basis during extreme rainstorm events, with higher average daily total edge weights indicating stronger human mobility during the event. The degree probability distribution of the network is the probability distribution or frequency distribution of the degrees of the nodes within the network, which serves as an indicator for assessing the importance of network nodes and the centrality of the network. The degree, daily average total edge weights, and the probability distribution of the degree of the mobile network are calculated as follows.

$$\text{Degree}(i) = \sum_j A_{ij} \quad (1)$$

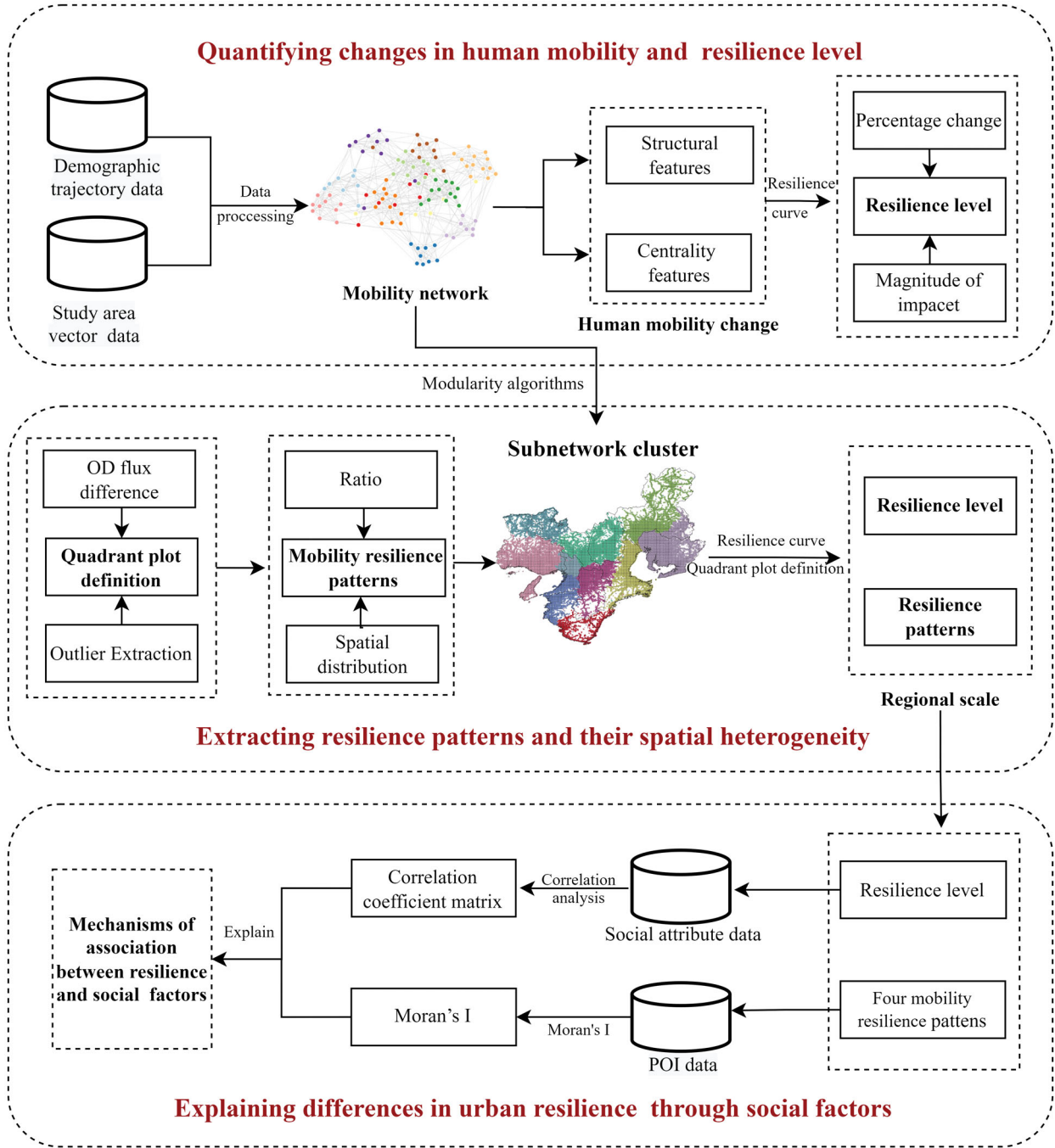


**Figure 2.** The proposed multiscale resilience computing framework on human mobility. It includes three interconnected parts: (1) analyzing spatiotemporal changes in human mobility and quantifying RLs, (2) extracting resilience patterns and their spatial heterogeneity, and (3) explaining differences in urban resilience through social factors. *Note:* OD = origin–destination; POI = point of interest.

$$T = \sum_{i=1}^N Degree_i \quad (2)$$

$$P(k) = C * k^{-\alpha} \quad (3)$$

where  $Degree(i)$  represents the degree of node  $i$ ;  $A_{ij} = 1$  if node  $i$  and node  $j$  are connected by an edge,

otherwise  $A_{ij} = 0$ ;  $T$  represents the total degree or total edge weight of the network;  $N$  is the total number of nodes in the network;  $P(k)$  is the probability of a node having a degree of  $k$ ;  $C$  is the normalization constant (ensuring the sum of probabilities is 1); and  $\alpha$  is the power-law exponent.

Afterward, we employ resilience curves to evaluate the RL of human mobility quantitatively. The resilience curve is composed of preevent, during-event, and postevent. The shape of the resilience curve and the duration required to achieve equilibrium after an event can measure a region's ability to recover from the impact of sudden incidents and ultimately achieve a new postevent equilibrium (Kontokosta and Malik 2018). As depicted in Figure 3, a typical resilience curve reflects the system behavior and describes continuous system performance levels before, during, and after an externally disruptive event (Meerow, Newell, and Stults 2016). The shaded regions demarcate the contours of performance loss. Accordingly, the RL can be calculated using the following equation.

$$RL = \frac{\int_{t_0}^{t_2} AP(t)dt}{\int_{t_0}^{t_2} NP(t)dt} \quad (4)$$

where  $t_0$  is the date of maximum impact,  $t_2$  is the time since reaching event equilibrium,  $RL$  is the human mobility resilience score,  $AP(t)$  is the actual score level, and  $NP(t)$  is the expected score level; that is, the total area under the dashed line. A-event is the maximum depth or maximum height of the resilience curve (Figure 3) to measure the extent of the impact of the contingency.

The specific calculation steps are as follows. First, we calculate the total edge weight of the network for each hour of the day. There are 264 data points during the full-length eleven-day observation window, twenty-four hours per day. It is assumed that the human activity before the event was not affected by the rainfall disaster and that the human movement was relatively stable. We take the average hourly OD flux from 30 May 2023 (hereinafter 5/30) to 1 June 2023 (hereinafter 6/1) as the preevent human activity level and set it as the preevent mobility performance benchmark. Subsequently, we define the percentage change in OD flux for the remaining period as the y-axis of the resilience curve. The formula for calculating this percentage change is as follows:

$$\text{Percentage change} = \left( \frac{p_i - p_0}{p_0} \right) * 100\text{percent} \quad (5)$$

where  $p_i$  is the total flux per hour per day and  $p_0$  is the average flux per hour before the event.

Then, this study uses a moving average algorithm to smooth and denoise the resilience curves. Ultimately, we normalize the data and calculate resilience scores using the definition of resilience scores in Equation 4.

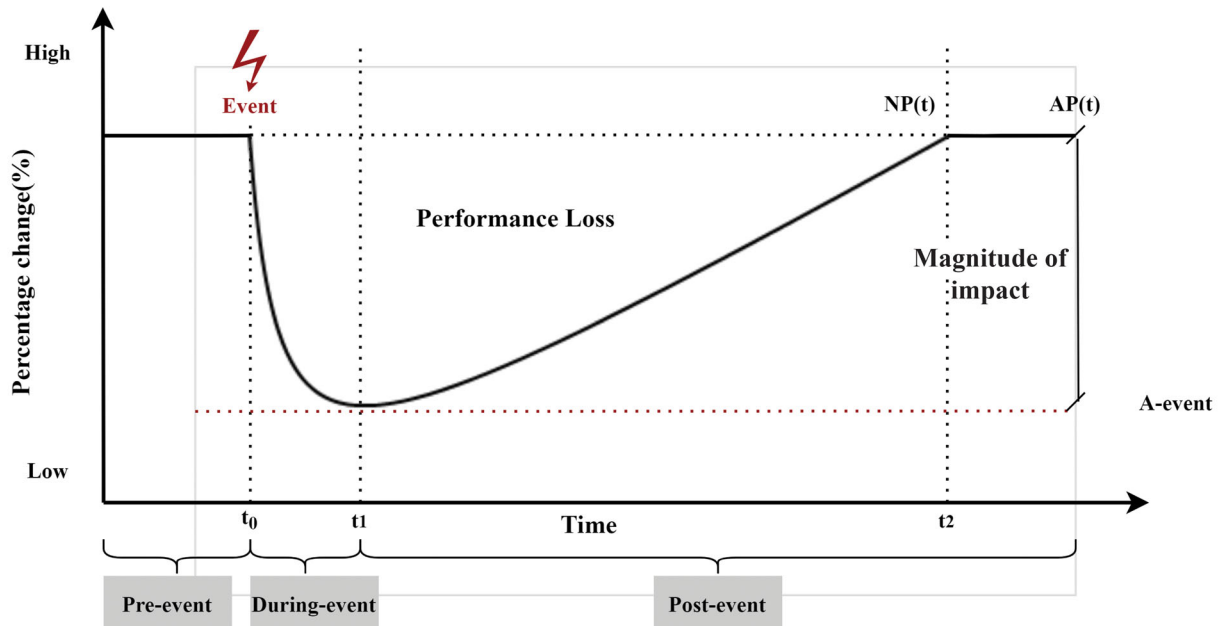


**Figure 3.** The demonstration of a typical resilience curve that reflects the temporal variation in the measurement of performance before, during, and after an externally disruptive event.



## Extracting Resilience Patterns and Their Spatial Heterogeneity

Because human mobility behavior under the cluster perspective is full of uncertainty and contingency, when confronted with extreme events, the travel behavior will show significant differences (Jia et al. 2019). These variances encompass route selection, the time they decide to travel, and their destinations. Consequently, the concept of human mobility resilience patterns delineates the adaptability and resilience exhibited by individuals amidst natural disasters, extreme weather phenomena, or emergent crises. In this study, it refers to the response of human mobility behavior to extreme rainstorm disasters. The paradigm of the resilience pattern is the classical bathtub-shaped resilience curve (or “drawdown-drawup” curve), also widely known as the resilience triangle model. This “down and up” view is the cornerstone of resilience-related research (Tang et al. 2023). As the performance level of a time series decreases when a disaster occurs, the difference between the preevent and during-event levels should be positive. Conversely, the performance curve rises gradually during the recovery process, and the difference between the levels during and after the event should be negative. By analyzing the drawdown-drawup performance of average daily flows in all spatial units, however, we find a large number of outliers in the falling and rising processes in both the outflow and inflow cases based on OD flux.

We employ a four-quadrant distribution plot to quantify various resilience patterns, analyze their spatial distribution, and extract outliers during the contraction and expansion phases. Initially, we calculate the daily average outflow and inflow in each  $1 \text{ km} \times 1 \text{ km}$  grid for all phases. The differences in flow volume from the preevent to the during-event phase and from the during-event to the postevent phase are used as the  $x$  and  $y$  coordinates. Based on the difference in the flow on the  $x$ -axis and  $y$ -axis, we convert the continuous values into right-angled coordinates to generate the four-quadrant distribution maps and to analyze the number and spatial distribution of each type of resilience pattern.

The complexity and large scale of urban agglomerations make it challenging to study and analyze them comprehensively and in-depth. Modularity algorithm is commonly used for optimizing the detection of community structures in networks. Nodes are categorized according to the connectivity

of the network, and nodes of the same type are added to the same clusters of subnetworks, which can be used for community discovery (Guo et al. 2022). Therefore, to analyze the changes in human mobility patterns at multiple spatial scales, this study uses a modularity algorithm to detect subnetwork clusters in a mobility network under normal conditions. We divide the spatial grids into different clusters to analyze the changes in urban resilience scores at the urban agglomeration scale and regional scales, respectively. These clusters also facilitate the exploration of variations in mobility patterns at smaller spatial scales, as calculated below:

$$Q = \frac{1}{2m} \sum_{ij} \left[ A_{ij} - \frac{k_i k_j}{2m} \right] \frac{s_i s_j + 1}{2} \quad (6)$$

where the number of edges between nodes  $i$  and  $j$  of the network is  $A_{ij}$ ;  $\frac{k_i k_j}{2m}$  is the desired number of edges between nodes  $i$  and  $j$ ;  $k_i$  and  $k_j$  are the vertex degrees; and  $m = \frac{1}{2} \sum_i k_i$  is the total number of edges in the network.

The Kolmogorov–Smirnov (K–S) distribution test is employed to assess the statistical significance of differences between clusters. It aids in inferring whether the two distributions are from the same source by comparing the frequency distributions of two samples or the magnitude of the difference between a sample’s frequency distribution and a particular theoretical distribution. In this study, we construct empirical frequency distribution functions by comparing outflow data across cluster grids. Subsequently, we compare these distributions to test whether the differences among clusters are statistically significant.

## Explaining Differences in Resilience Patterns through Social Factors

POI data link human activities with locations by portraying the dynamics and real-time nature of urban land use (Gong et al. 2020), which provide a new research perspective in terms of intracity spatial structure and functional division, intercity interactions, and so on. The spatial distribution of POIs can reflect an area’s functional characteristics and is closely related to the behavioral patterns and lifestyles of the population. It can also provide insights into how well different areas are equipped to support humans during crises, thereby directly linking

resilience patterns to urban functionality and service provision. Thus, this study uses a bivariate-based spatial autocorrelation approach to analyze the mutual influence and nuanced relationships of these two spatial phenomena. The bivariate-based local spatial autocorrelation has high applicability in describing the spatial correlation and dependence characteristics of two geographical elements. The Moran's  $I$  ( $I^{ab}$ ) value ranges from  $-1$  to  $1$ , with positive, negative, and  $0$  values indicating positive, negative, and no correlation, respectively. The larger the absolute value, the stronger the spatial autocorrelation (Shi et al. 2023). We first build fishing nets within each subnetwork cluster in the study area. After that, we spatially correlate the POI data with each subnetwork cluster, enumerate the density of each type of POI in each subnetwork cluster, and establish the spatial distribution of the POIs. Then, we use Geoda software to conduct a bivariate Moran's  $I$  analysis based on empirical Bayesian ratios for the spatial distribution of resilience patterns and POIs. Based on the distance relationship, we create a spatial weight matrix and calculate Moran's  $I$ . This enables us to investigate the relationship between the distribution of resilience patterns and the spatial distribution of POIs.

$$EBI^{ab} = X_i^a \sum_{j=1, j \neq i}^n w_{ij} X_j^b \quad (7)$$

where  $X_i^a$  and  $X_j^b$  are the values of variables  $a$  and  $b$  at positions  $i$  and  $j$ , respectively;  $EBI^{ab}$  is the local Moran's  $I$  based on empirical Bayesian ratios at position  $i$ ; and  $w_{ij}$  is a spatial weight matrix weighted based on the distance between positions  $i$  and  $j$ .

Furthermore, income level serves as a key indicator of economic capacity, and insurance coverage reflects residents' risk management abilities. Both are commonly used in urban resilience research as core measures of economic resilience (Yu et al. 2024). The proportion of the elderly population highlights social vulnerability, and the gender ratio reflects demographic resilience. Collectively, these indicators offer a more comprehensive assessment of urban resilience (Petaroli and Baars 2022; Yu et al. 2024). Therefore, we select per-capita income (PCI), age 65+ (percentage of the population over age sixty-five), males (percentage of male population), females (percentage of female population), and insured (percentage of insured individuals) to investigate the relationship between human mobility resilience and urban social factors. The results are presented in the

form of correlation coefficient matrix heat maps. Given samples  $x_1, x_2, \dots, x_n$  from a normal population  $N_p(\mu, \sigma^2)$  of capacity  $n$ , calculate the correlation coefficients  $r_{ij}$  between the two samples, respectively:

$$r_{ij} = \frac{\sum (x - \bar{x})(y - \bar{y})}{\sqrt{\sum (x - \bar{x})^2 \sum (y - \bar{y})^2}} \quad (8)$$

where  $r_{ij}$  is the correlation coefficient, and  $\bar{x}$  is the sample mean.

## Results

### Assessment Results of Resilience Levels of Population Groups

Extreme rainfall events simultaneously reduce the overall intensity of population movement and the number of critical nodes in the mobility network during the event. We construct the mobility network based on human mobility data. As shown in Figure 4, the number of network edges and the total edge weights initially decrease, then increase, and eventually stabilize, illustrating that human mobility during the rainfall event showed an overall trend of decreasing and then increasing. According to JMA, on 2 June 2023 (hereinafter 6/2), the maximum rainfall occurred in the study area under the influence of Typhoon Mawar, which directly led to a decrease in foot traffic. Consistent with the fluctuation in Figure 4, the number of network edges and the total edge weight plummeted on 6/2. On 6/2, some trains on the Tokaido Shinkansen were suspended for the day, and some other interdistrict trains were delayed to varying degrees. This event suggests that the overall intensity of human mobility was reduced, which might have been due to factors such as traffic disruption, waterlogged roads, and the suspension of public transport as a result of the heavy rainfall.

As shown in Figure 5, the network's distribution degree is affected by the apparent spacing in the tails between the distribution during the event and the distributions of the other two phases. When the nodes have the same degree, the probability distribution of the during-event phase has smaller values and fewer larger nodes. This result also indicates a reduction in the number of larger critical nodes in the network, which suggests that the functioning of essential human-gathering places or key transport hubs was limited during the disaster. Nonetheless,



**Figure 4.** Temporal changes in the total edge weights and the edge numbers of the network within the observation window. Here, the total edge weights represent the total origin–destination flux, and the edge numbers represent the degree of connectivity between the grids.

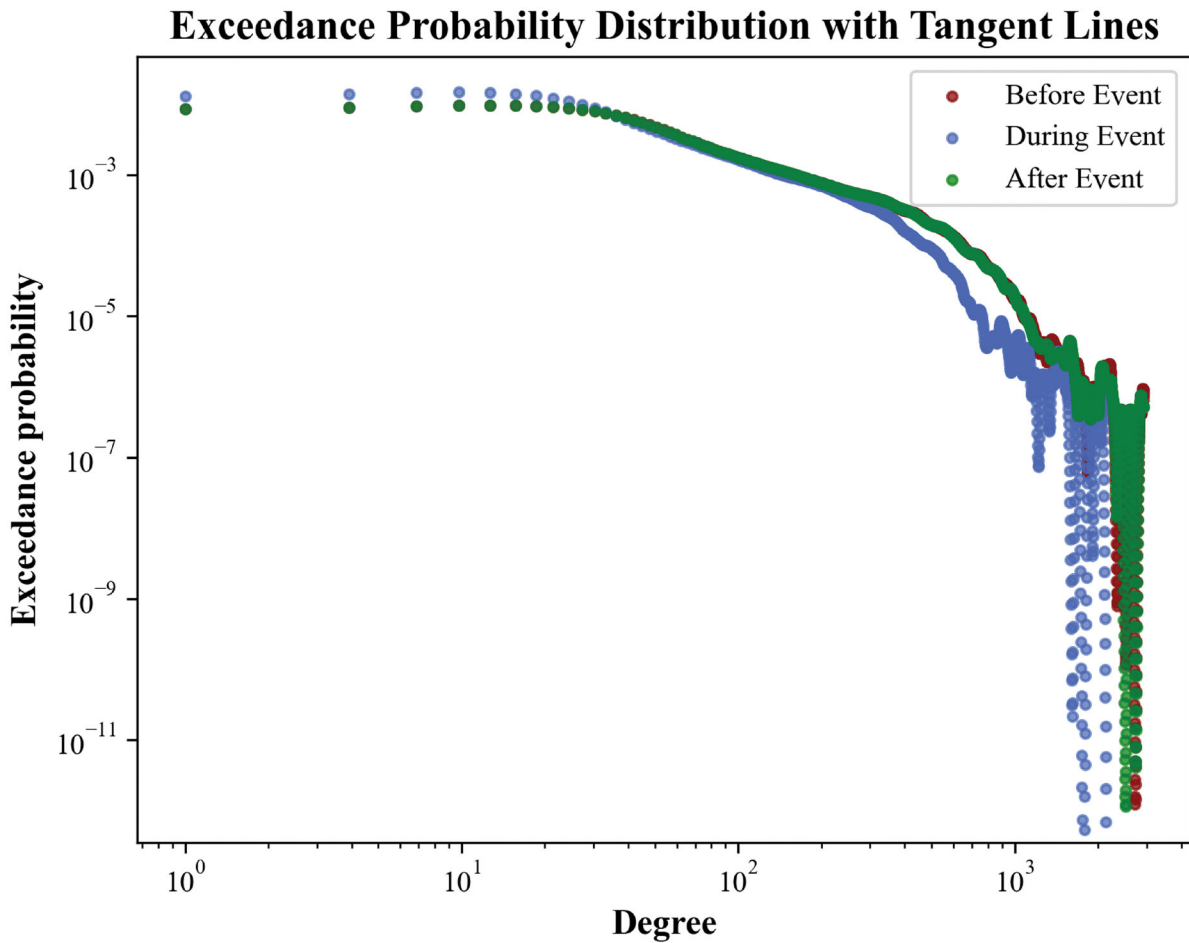


**Figure 5.** Probability distribution of the network degree for the three phases of the event. The horizontal axis represents the network degree, the vertical axis represents the exceeding probability distribution of the network nodes, and the tails are apparently spaced between the distribution during the event and the other two phases.

the slopes of the curves in the power law distribution did not change drastically in the different event phases, suggesting that the primary nodes within the network maintain relative stability. This phenomenon means that rainfall disasters primarily lead to a decrease in the overall intensity of mobility rather than radically reducing the connectivity of peripheral areas in the network.

We calculated the mobility resilience score using the resilience curve definition and statistical tests. We set the average hourly OD flux from 5/30 to 6/1 (i.e., three consecutive days prior to the disaster) as the preevent mobility performance baseline and converted the mobility flux to a percentage change. Owing to the curve's rebound during the event, we employed linear interpolation to segment the area between the curve and the axes. We then calculated and obtained a quantitative score of 0.59 for the resilience of human mobility for the entire urban agglomeration, in contrast to the regional resilience score afterward. This result suggests that despite the short-term impacts of disasters on urban mobility, human mobility networks remain quite resilient and gradually recover their functions after disasters. The findings hold significant implications for comprehending urban resilience and refining disaster response strategies (Figure 6).

### Multiple Resilience Patterns for Disaster Response

The classic resilience curves show a drawdown-drawup pattern of human flows, but we found many abnormal patterns during this rainfall event. We mapped the pattern of human mobility onto a quadrant map, revealing four different types of resilience patterns (Figure 7). The typical resilience pattern is a bathtub-shaped resilience pattern, which is located in the fourth quadrant, accounting for about 42 percent of the total. Conversely, the other three abnormal types of resilience patterns are the decreasing pattern, reversed bathtub-shaped pattern, and increasing pattern, which are located in the first, second, and third quadrants, accounting for about 14 percent, 31 percent, and 8 percent of the total patterns, respectively. The ratio of these four resilience patterns from the first to the fourth quadrant is approximately 1:4:1:4. It is noteworthy that the prevalence of these abnormal resilience patterns is unexpectedly high, with the ratio of classical to abnormal resilience patterns standing at approximately 2:3. This observation suggests that our traditional understanding of resilience patterns might be insufficient in capturing the complexity of humans' adaptive responses when faced with sudden-onset disasters.

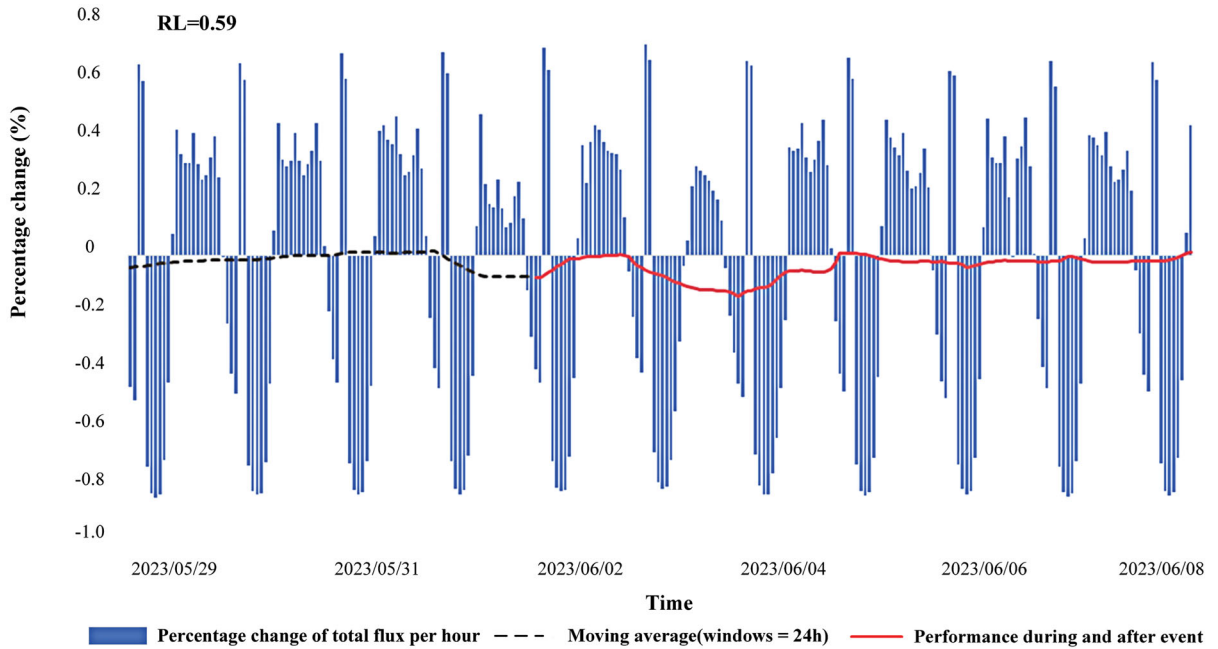


**Figure 6.** Urban agglomeration resilience metric. The total flux is defined as the total edge weight of the network at each hour, with the dotted and solid lines representing moving averages based on the normalized percentage change in mobility performance from the preevent baseline. *Note:* RL = resilience level.

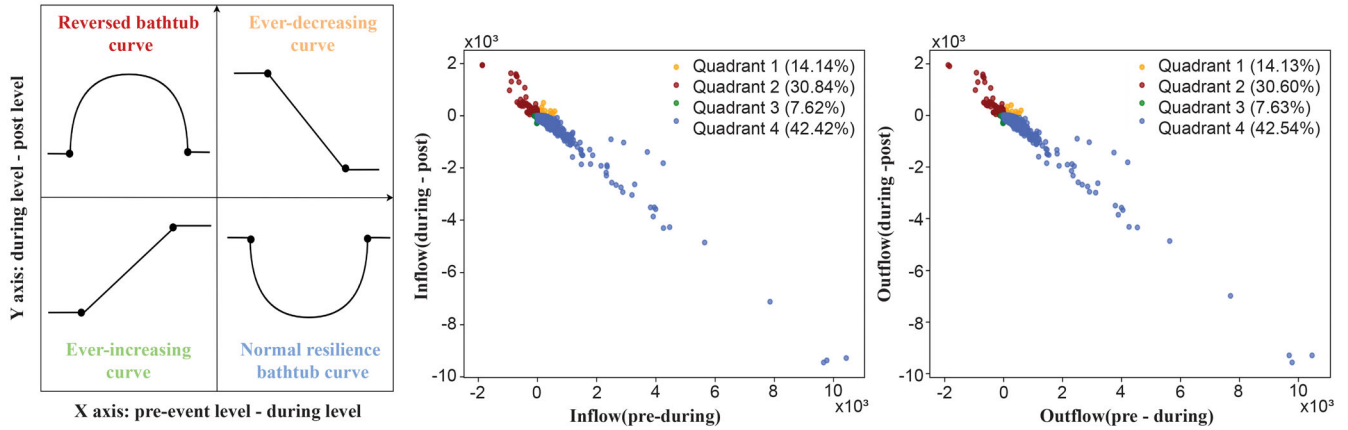


**Figure 7.** Quadrant distribution of origin–destination inflow and outflow resilience patterns. (A) Definition of the four different types of resilience patterns found within urban agglomerations. (B, C) Quadrant distribution of inflow and outflow resilience patterns.

In Figure 8, there are only minor differences in the spatial distribution of OD inflows and outflows, which are approximately equally distributed. Classical recovery patterns (i.e., blue spots) are uniformly dispersed across the study area. In contrast, increasing and decreasing resilience patterns are located around the periphery of the reversed bathtub recovery patterns (i.e., red spots), forming narrow corridors and minor agglomerations. In Figure 7B and C and Figure 8, in the case of outflows, the bathtub-shaped resilience pattern ( $\sim 42$  percent) suggests that the high mobility inflow of humans diminishes to lower levels during the preevent impact phase, potentially reflecting people’s disaster avoidance behavior and returning to these locations or regular routes after the event. It is also possible that people moved to shelters for survival and safety and returned to their place of residence after the disaster. The increasing pattern ( $\sim 8$  percent) suggests that population inflows to these places were stimulated during the rainfall, and the increasing trend continued during the recovery phase after the event. One possible explanation is that individuals established and maintained new habits after the disaster. In addition, in areas that were heavily affected, frequent interactions between relief workers and affected residents might have occurred, which led to an increase in foot traffic over an extended period. Conversely, a decreasing pattern ( $\sim 14$  percent) suggests that the rainfall dampened inflows to the region and that this trend of decreasing continues after the disaster. This observation indicates that disaster events lead to tourists’ persistent avoidance of affected areas in the postdisaster period. This

behavioral pattern is likely influenced by considerations of personal safety and the extent of infrastructural damage.

In addition, we have found that the greater the human flow intensity at a location before rainfall, the higher the likelihood of an unusual recovery pattern during a disaster. Figure 8 (A1, A2, B1, B2) illustrates Osaka City and Nagoya, both of which are essential administrative, economic, and transportation hubs with a vast number of daily commuters. It also depicts Kyoto (A3, B3), a significant tourist destination in Japan with a substantial daily influx of people. In such high pedestrian traffic areas, we observe that human behavior undergoes more pronounced change during disaster occurrences. People could exhibit more urgent, chaotic behavior, leading to a higher probability of abnormal resilience patterns. This finding inspires us to explore further the causes and impacts of this abnormal resilience pattern at regional scales to guide managers in developing more effective disaster management strategies.

### Analysis of Subnetwork Clustering Based on Different Resilience Patterns

We employed a modularity algorithm to detect ten clusters (subnetwork clusters) in the human mobility network during the preevent phase at resolution = 2, categorizing the spatial grid into different clusters. As shown in Figure 9, the administrative boundaries of the regions within the city cluster are roughly similar to the boundaries of the subnetwork clusters obtained by the community detection method. This significant spatial coupling indicates



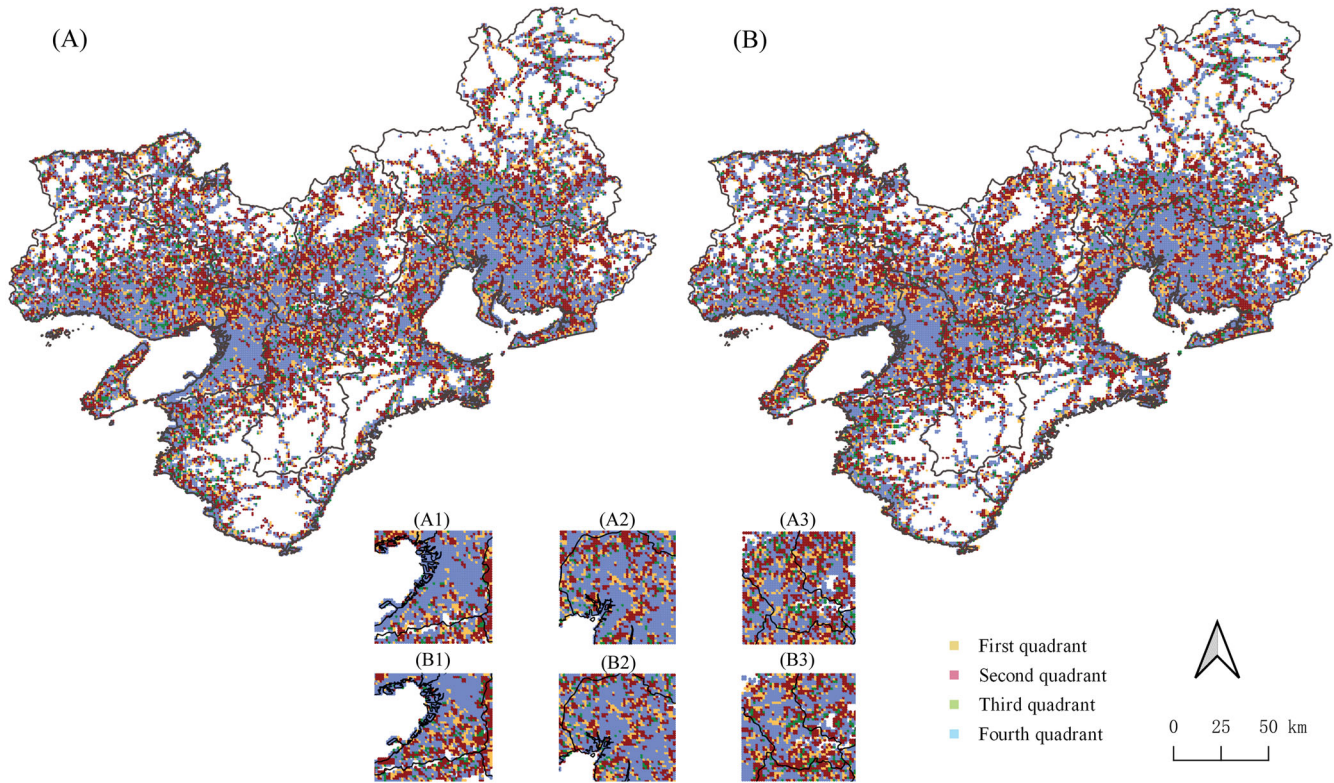


**Figure 8.** (A) Spatial distribution of inflow resilience patterns of origin–destination (OD) movement. (B) Spatial distribution of outflow resilience patterns of OD movement. A1 through A3 and B1 through B3 are the spatial distributions of inflow and outflow resilience patterns in Osaka City, Nagoya, and Kyoto, respectively.

that most human mobility activities are localized within administrative boundaries, with relatively few movements across clusters.

We employed the K–S test to delineate disparities in outflow distributions across the ten clusters. The results show the difference distribution within clusters is statistically significant, as detailed in Table 1. The A-event column is the maximum depth value of the resilience curve, indicating the degree to which the disaster event influenced human mobility. The A-event values for Clusters 3, 6, and 10 are  $-0.199$ ,  $-0.168$ , and  $-0.146$ , respectively, with larger absolute values, indicating that Clusters 3, 6, and 10 are the most affected on average by this extreme rainfall event. As per the data released by Japan’s Ministry of Internal Affairs and Communications Statistics Bureau, Clusters 6 and 10 registered casualties of three and five individuals, respectively. Furthermore, Cluster 6 reported damage to approximately 1,180 households, marking an extremely severe impact of the rainstorm. Additionally, the resilience scores of each cluster range from 0.30 to 0.70, with an average resilience score of 0.49. The RL differs from the resilience score of 0.56 for the whole city cluster derived

in the previous section, which could be related to the population density, infrastructure, and economic level of each region among the clusters.

As depicted in the first row of Figure 10, the ratios of the four resilience patterns, namely the decreasing pattern, reversed bathtub-shaped pattern, increasing pattern, and bathtub-shaped pattern, in the four quadrants of Clusters 1, 2, 4, 5, 6, 8, and 9 are primarily close to the ratio of 1:4:1:4 on the scale of urban agglomerations. The ratio of the normal resilience pattern (i.e., Quadrant 4) to the abnormal resilience pattern (i.e., Quadrants 1, 2, and 3) in each cluster is about 2:3. This observation suggests the stability of a resilience pattern at both the urban agglomeration scale and the regional scale. As shown in the second row of Figure 10, the spatial distribution of each resilience pattern is roughly consistent with the urban agglomeration scale. The normal resilience pattern is evenly distributed, whereas abnormal patterns show narrow corridors and a small agglomeration distribution. Based on the obtained spatial distribution results of each cluster resilience pattern, we also explore its relationship with the spatial distribution of POI in the following study. Using

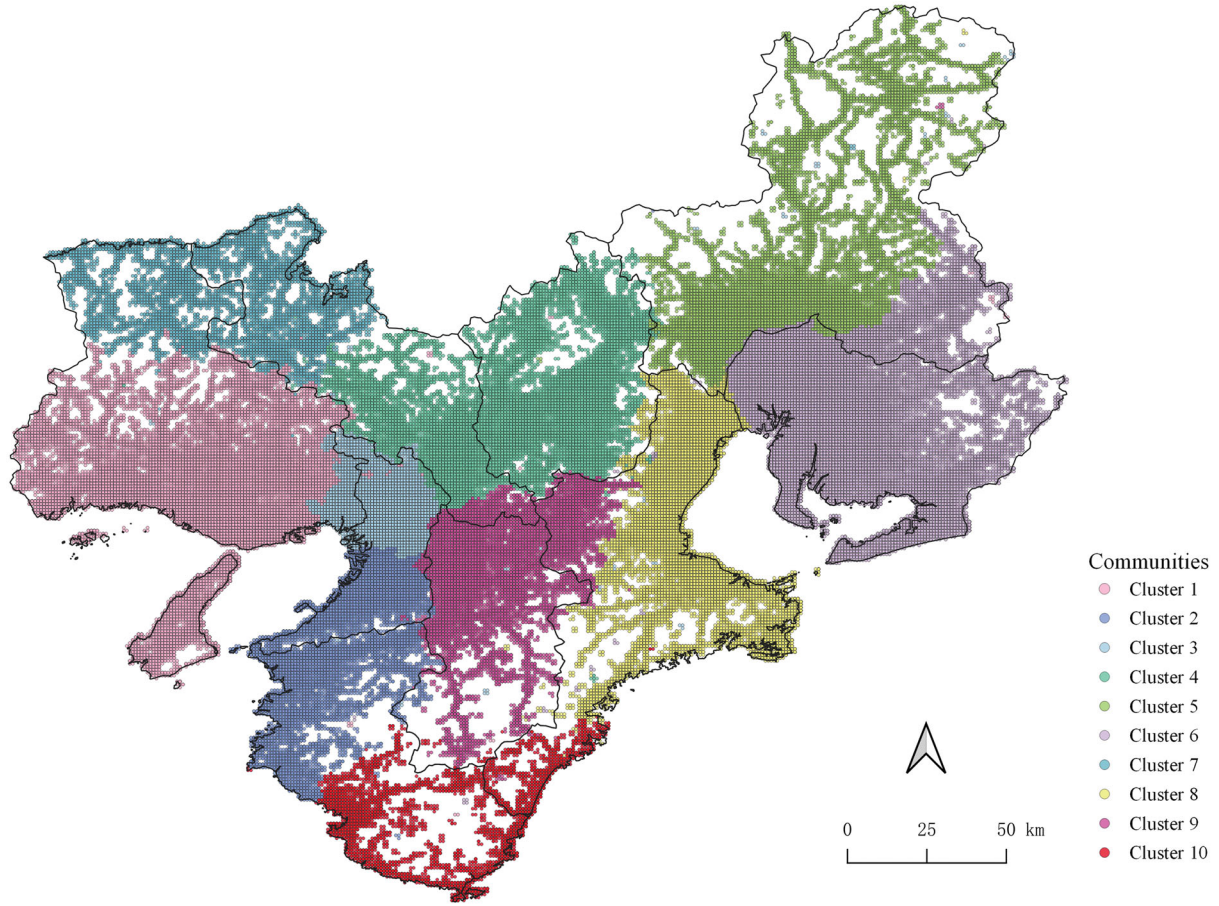


**Figure 9.** Cluster detection for mobility networks in the preevent phase. Different colors mark the ten different main clusters.

**Table 1.** Description of the outflow mobility

Cluster	Basic attribute size (grid count)	Description		Test of normality (Kolmogorov–Smirnov)		
		Resilience level	A-event	Statistic	df	Significance
1	5,691	0.46	−0.114	0.343	5,542	0.000
2	2,891	0.55	−0.102	0.307	3,291	0.000
3	1,253	0.56	−0.199	0.328	1,704	0.000
4	5,000	0.49	−0.106	0.306	2,804	0.000
5	5,030	0.49	−0.091	0.265	1,244	0.000
6	6,286	0.59	−0.168	0.297	4,817	0.000
7	3,161	0.37	−0.107	0.261	4,812	0.000
8	3,663	0.42	−0.062	0.298	6,131	0.000
9	3,401	0.45	−0.077	0.275	3,028	0.000
10	1,836	0.57	−0.146	0.281	3,559	0.000

the resilience curves of each cluster (the third row in Figure 10) and the definition of the resilience score formula, we calculated the RLs for all ten clusters, with the results presented in Table 1. The resilience curves for the individual clusters reveal that

each cluster experienced significant or slight decreases in normal activity levels during and after the event. Until the end of the observation period, none of the ten clusters had fully reverted to its pre-event levels.

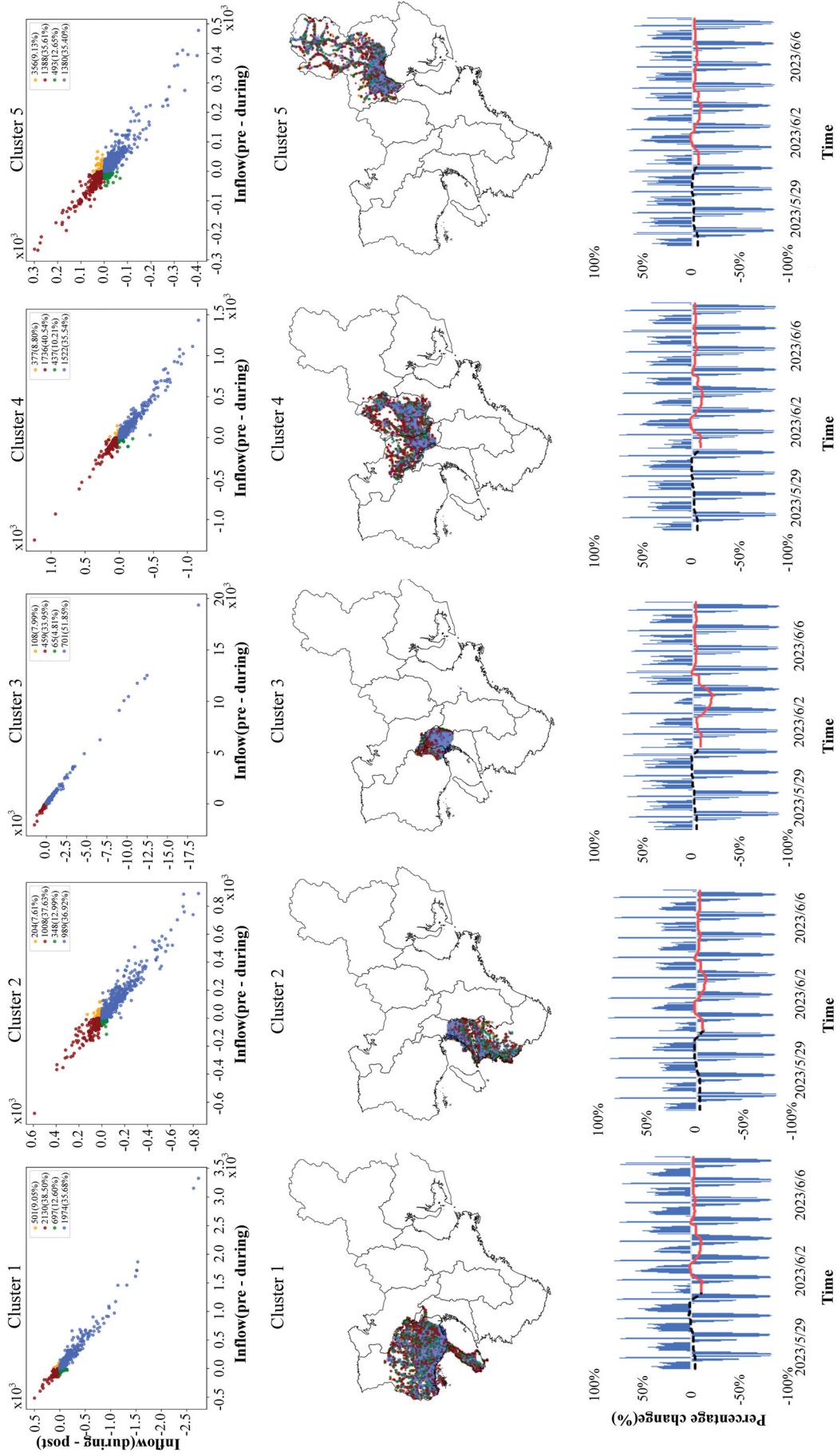


Figure 10. Quadrant, spatial distribution, and resilience curve of resilience patterns by cluster. The first row represents the quadrant distribution of resilience patterns. The second row represents spatial distribution resilience patterns of origin–destination movement. The third row represents resilience curves for ten clusters.



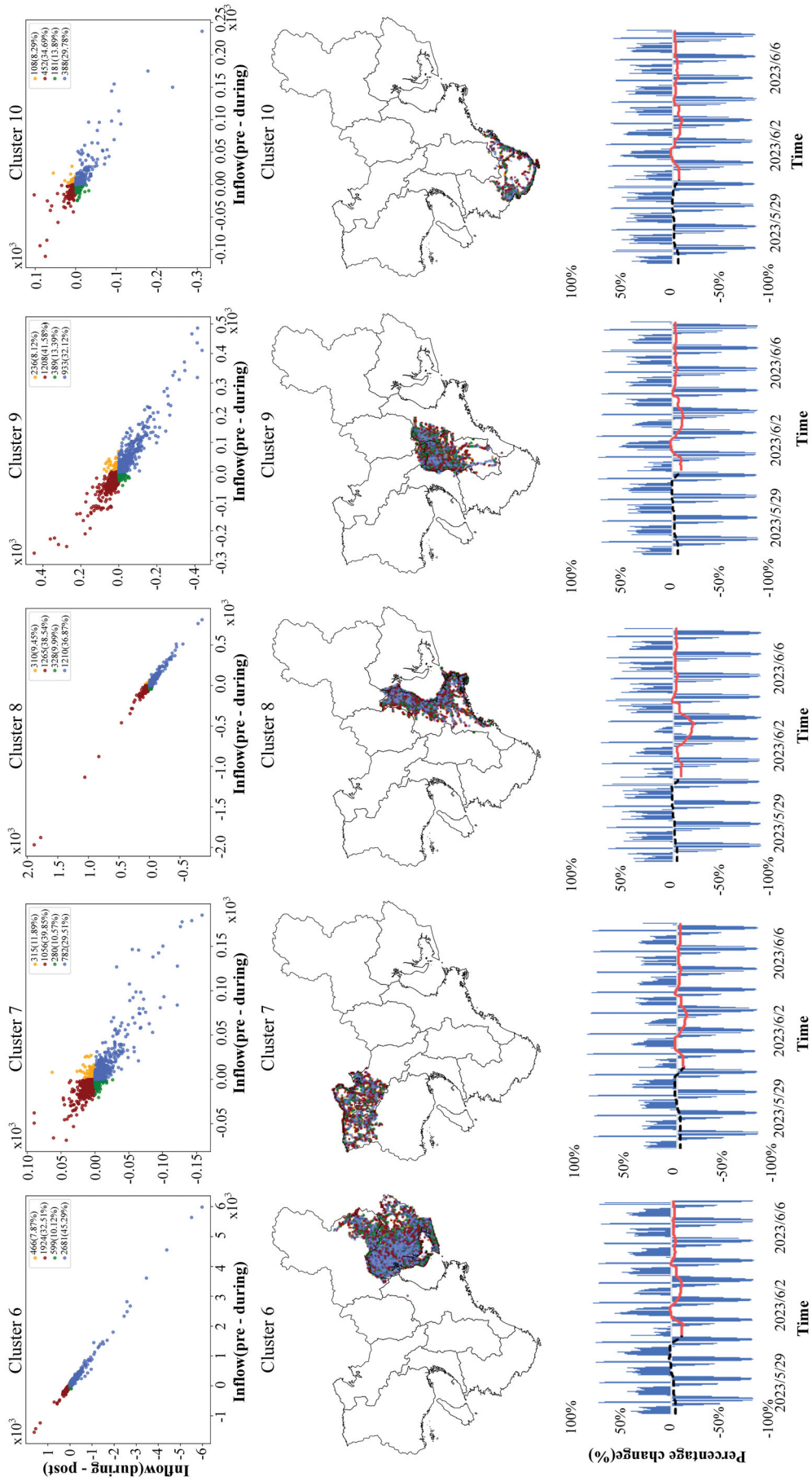


Figure 10. Continued.

### Analysis of Social Factors Influencing Abnormal Resilience Patterns

The spatial distribution of POIs can reflect the functional characteristics of an area and is closely related to the behavioral patterns and lifestyles of the population. Table 2 presents the EBI estimates (bivariate Moran's I calculated using empirical Bayesian ratios, as defined in Equation 7) of the spatial distribution of various types of POIs and resilience patterns and their significance test results. None of the EBI estimates is zero, and the absolute values are large. Meanwhile, all Z values surpass the acceptance threshold of 1.96 at the 95 percent confidence level of the normal distribution. This suggests that there is a better spatial correlation between POI and the distribution of resilience patterns in the study area. The various resilience patterns are closely related to the built environment with different geographical contexts.

The EBI values between the decreasing resilience patterns and POIs' distribution for tourism, recreation, food and beverage, commerce, construction, education, transportation and logistics, and hotel accommodation are all greater than 0.40, with a high positive correlation. There is a decreasing trend in the observation window, indicating that all types of industries have been affected by rainfall for a longer period and have not recovered. For the reversed bathtub-shaped resilience pattern, the EBI value with the recreation POI distribution is  $-0.013$ , whereas the EBI values with other POIs' distributions are all positive. These results indicate an absence of increased foot traffic in the recreation areas during disaster events. The bathtub-shaped resilience pattern exhibits positive EBI values in relation to all types of POI distributions, consistent with earlier findings that normal resilience patterns are uniformly distributed within the study area.

Moreover, recreation, tourism, and other areas with high daily foot traffic all have high correlations with the distribution of abnormal resilience patterns. These findings are consistent with previous results, suggesting that abnormal resilience patterns are more likely to be concentrated in grids with higher pre-event daily average fluxes. These findings help us understand the relationship between different resilience patterns and urban functions and various sectors, as well as how the human flow in various urban functional areas changes during disasters and post-disaster recovery. Tailored emergency strategies and

**Table 2.** Point of interest distribution and EBI estimates for resilience patterns (decreasing pattern, reversed bathtub-shaped pattern, increasing pattern, and bathtub-shaped pattern are named as abnormal resilience patterns 1, 2, 3, and normal resilience pattern)

		Tourism and sightseeing	Transportation and logistics	Recreation and entertainment	Hotel and accommodation	Food and beverage	Commerce	Education	Construction
Abnormal pattern 1	EBI	0.549	0.438	0.640	0.415	0.575	0.596	0.524	0.666
	Var (EBI)	0.006	0.017	0.015	0.016	0.020	0.013	0.017	0.017
	p	0.001	0.001	0.001	0.001	0.001	0.001	0.001	0.001
	Z	89.696	25.884	41.516	25.393	28.636	45.308	32.616	39.874
Abnormal pattern 2	EBI	0.323	0.291	-0.013	0.161	0.387	0.437	0.405	0.581
	Var (EBI)	0.008	0.009	0.016	0.007	0.008	0.008	0.001	0.001
	p	0.001	0.001	0.001	0.001	0.001	0.001	0.009	0.001
	Z	40.512	34.242	7.886	21.844	47.808	52.085	47.249	69.795
Abnormal pattern 3	EBI	0.027	0.330	0.332	0.801	0.361	0.379	0.461	0.640
	Var (EBI)	0.002	0.029	0.027	0.013	0.016	0.027	0.029	0.029
	p	0.001	0.001	0.001	0.001	0.001	0.001	0.001	0.001
	Z	16.376	11.330	12.135	0.206	23.400	14.279	15.947	22.316
Normal pattern	EBI	0.407	0.495	0.292	0.331	0.405	0.576	0.479	0.685
	Var (EBI)	0.025	0.006	0.006	0.007	0.006	0.006	0.007	0.007
	p	0.001	0.001	0.001	0.001	0.001	0.001	0.001	0.001
	Z	16.612	78.995	50.607	51.145	3.249	101.717	73.646	104.643

Note. EBI = the bivariate Moran's I calculated using empirical Bayesian ratios, as defined in Equation 7.



disaster risk management can be proposed for each sector, thereby improving the adaptive capacity during disasters.

This study uses correlation analysis to explore the relationship between the levels of mobility resilience (as shown in the resilience level in Table 1) and urban social factors across various population clusters. As illustrated in Figure 11, a robust positive correlation is evident between PCI and RL, with a correlation coefficient of 0.42. This finding suggests that regions with higher income levels might possess a better capacity to handle assorted challenges and pressures. The correlation coefficient between the proportion of individuals age sixty-five and above and the level of resilience is approximately  $-0.18$ , indicating that a higher percentage of older individuals corresponds with a lower level of resilience. The correlation coefficients between gender

differences (males/females) and RLs are the smallest, at  $0.16$  and  $-0.16$ , respectively, suggesting that gender exerts a relatively minor influence on RLs. The higher proportions of males are associated with relatively higher levels of resilience, whereas the opposite is true for females. Furthermore, the coefficient of correlation between the number of insured and the level of resilience is  $0.50$ , which implies that in areas with a greater number of insured persons, the social and economic system is more likely to provide support and security, thus increasing the level of resilience.

The positive correlation between the level of PCI and insurance coverage and the level of resilience is the most significant, suggesting that economic development and the improvement of the social security system are the keys to enhancing urban resilience. The effects of population aging and gender

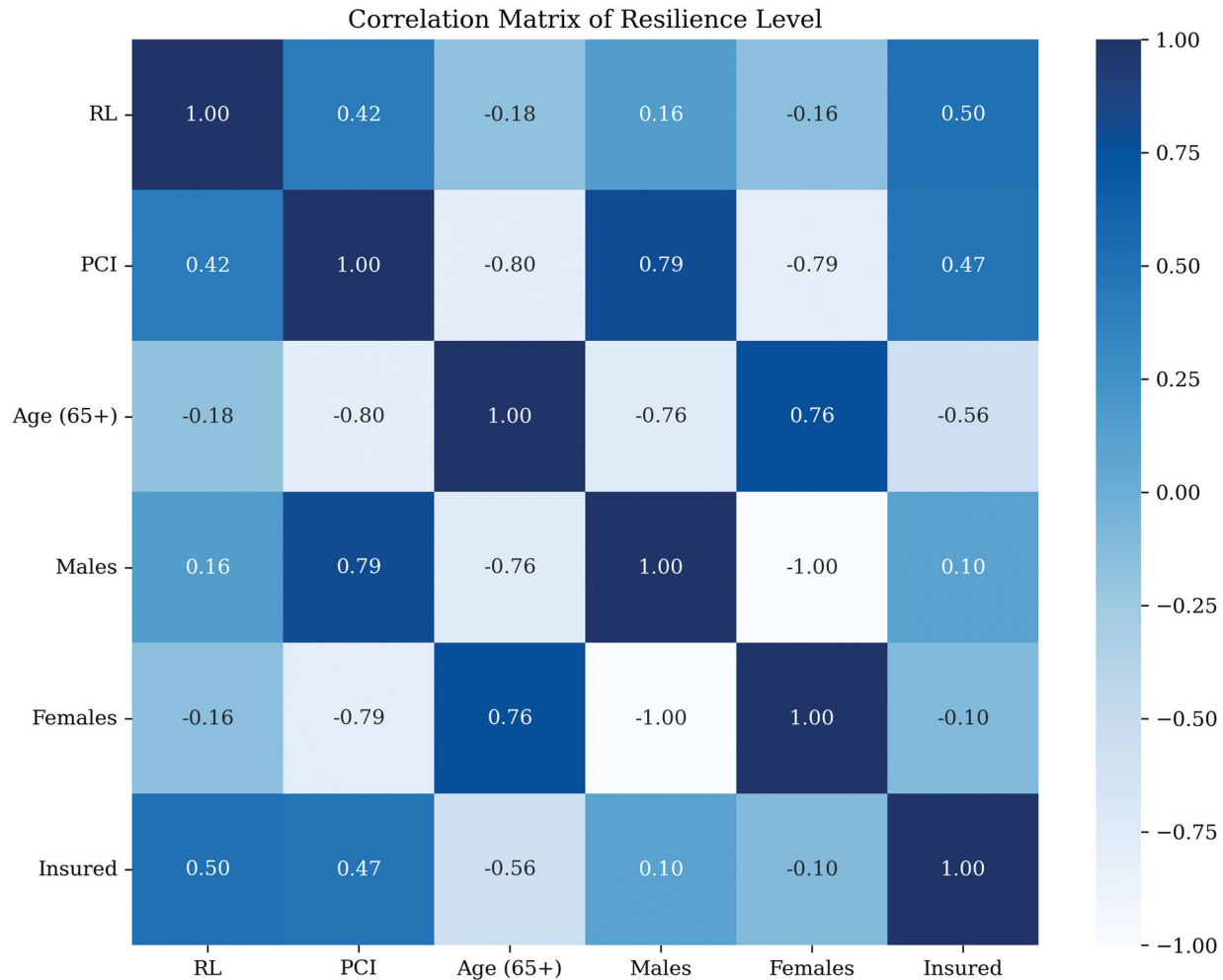


**Figure 11.** Matrix of correlations of resilience levels (RLs) of population groups. *Note:* PCI=per-capita income; age (65+) = share of population older than sixty-five; Males=share of male population; Females=share of female population; Insured=share of number of insured persons.

differences on the RL, although relatively small, should not be ignored and need to be dealt with through comprehensive measures.

## Discussion

This study comprehensively assesses the resilience levels and patterns of multiscale human mobility within two major urban agglomerations in Japan during extreme rainfall events. It solves the problem of the lack of exploring the distribution rule of mobility resilience patterns and its causes in the existing studies at multiple scales. Furthermore, it provides a new reference for better understanding the complexity of collective movement behavior of high-density populations under extremely hazardous weather conditions.

### Interpretation of the Findings

Based on a mobility network generated from large-scale trajectory data, the constructed urban agglomeration resilience assessment system accurately assesses the ability of regions to withstand and recover from destructive events. Sudden disasters and shocks can significantly alter human travel behavior (Haraguchi et al. 2022; Yao et al. 2023). For example, human activity levels shown in the cluster resilience curves have decreased, highlighting the challenge of returning resilience to preevent disaster levels. X. Zhang and Li (2022) found that extreme disasters cause movement perturbations among individuals to show significant differences. Similarly, our study also found a large number of abnormal resilience patterns in human mobility, and the ratio of abnormal to normal resilience patterns is about 3:2. Heavy rainfall does not occur simultaneously, at identical locations, or with uniform intensity across the study area, resulting in varied response times and uneven infrastructure damage throughout the built environment. This variability prompts individuals to react differently to events across diverse geographic environments, thereby manifesting different mobility resilience patterns. This finding suggests that the actual impacts of this heavy rainfall event might exhibit greater variability at the microlevel. For policymakers, it is crucial to pay attention to areas exhibiting abnormal resilience patterns, as these could indicate potential long-term changes in land use. Emergencies can cause a sudden surge in resource demand to accommodate population gatherings. Disasters could damage

roads, bridges, and other transportation facilities, disrupting normal transportation patterns and forcing people to find new routes or modes of transportation. In such emergencies, governments should implement reasonable contingency measures to maintain critical infrastructure functioning and provide emergency services to meet essential population needs.

With further global warming and rapid urban development, urban rainfall patterns are changing, leading to an increase in the frequency and intensity of rainfall events. Extreme precipitation is becoming the norm, posing significant challenges to built and natural environments. This study provides a methodology to quantify urban resilience under different rainfall patterns by analyzing the changes in human mobility. By exploring the relationship between different POI categories and resilience patterns, this study can capture whether urban functional areas or industries face sudden increases, decreases, or no change in human mobility during extreme weather events. These insights are instrumental in formulating targeted disaster prevention and mitigation strategies, including optimizing evacuation routes or developing specialized recovery strategies for specific areas. In addition, the method proposed provides valuable insights into the vulnerability and potential risks faced by the built environment. It can help cities to better adapt to changing climatic conditions and reduce the impact of extreme weather events on the lives and property safety of urban residents.

### Analysis of Factors Affecting Urban Resilience and Recommendations for Disaster Management

Previous research has highlighted considerable disparities in disaster response behaviors and resilience among communities distinguished by demographic and socioeconomic characteristics (Hong et al. 2021; Smiley et al. 2022). In this study, we propose to use the spatial distribution of POIs for the first time to elucidate the relationship with the distribution pattern of resilience patterns. Our findings indicate a close correlation between the spatial distribution of resilience patterns and local geographical settings within the built environment. Additionally, we observe different behaviors of population groups with different demographic and socioeconomic characteristics, highlighting pronounced disparities and inequalities. Inequality is more severe and pronounced among socially disadvantaged groups, such

as those with low economic levels and an aging population. Hence, this research can equip government policymakers with novel insights into the disparities among various groups across different geographies, enabling them to take action to support disadvantaged areas. Priority should be given to the equitable distribution of resources and the optimization of urban infrastructure to accommodate the needs of different population groups; reducing inequalities and increasing the urban population resilience as a whole, especially in communities with lower socio-economic status, more advanced aging, and so on; optimizing shelter locations and evacuation routes; conducting outreach to at-risk populations; and assisting more vulnerable areas or population groups.

It is noteworthy that our findings indicate the probability of abnormal mobility resilience patterns during a disaster is higher in areas with high daily human flow, such as Osaka, Nagoya, and Kyoto. This finding underscores the importance of tailored disaster management strategies for different regions.

For the tourist city of Kyoto, special evacuation plans need to be developed, considering the unfamiliarity of tourists with local evacuation routes and shelters. For instance, creating easily accessible evacuation maps and ensuring the presence of emergency kits at major tourist sites like Kinkakuji and Kiyomizu-dera can significantly enhance preparedness. Regular drills and training sessions for local personnel and volunteers are also crucial for ensuring efficient evacuation procedures. In central cities like Osaka and Nagoya, effective traffic control is required during the disaster. Depending on the disaster type and the extent of its impact, multilevel traffic diversions are implemented to ensure the rapid movement of rescue teams and the orderly evacuation of residents. For commercial areas, encouraging adaptive building designs, such as adjustable drainage systems, can help mitigate the impact of varying rainfall levels. In addition, public safety and disaster education need to be strengthened to ensure that residents and visitors alike understand how to

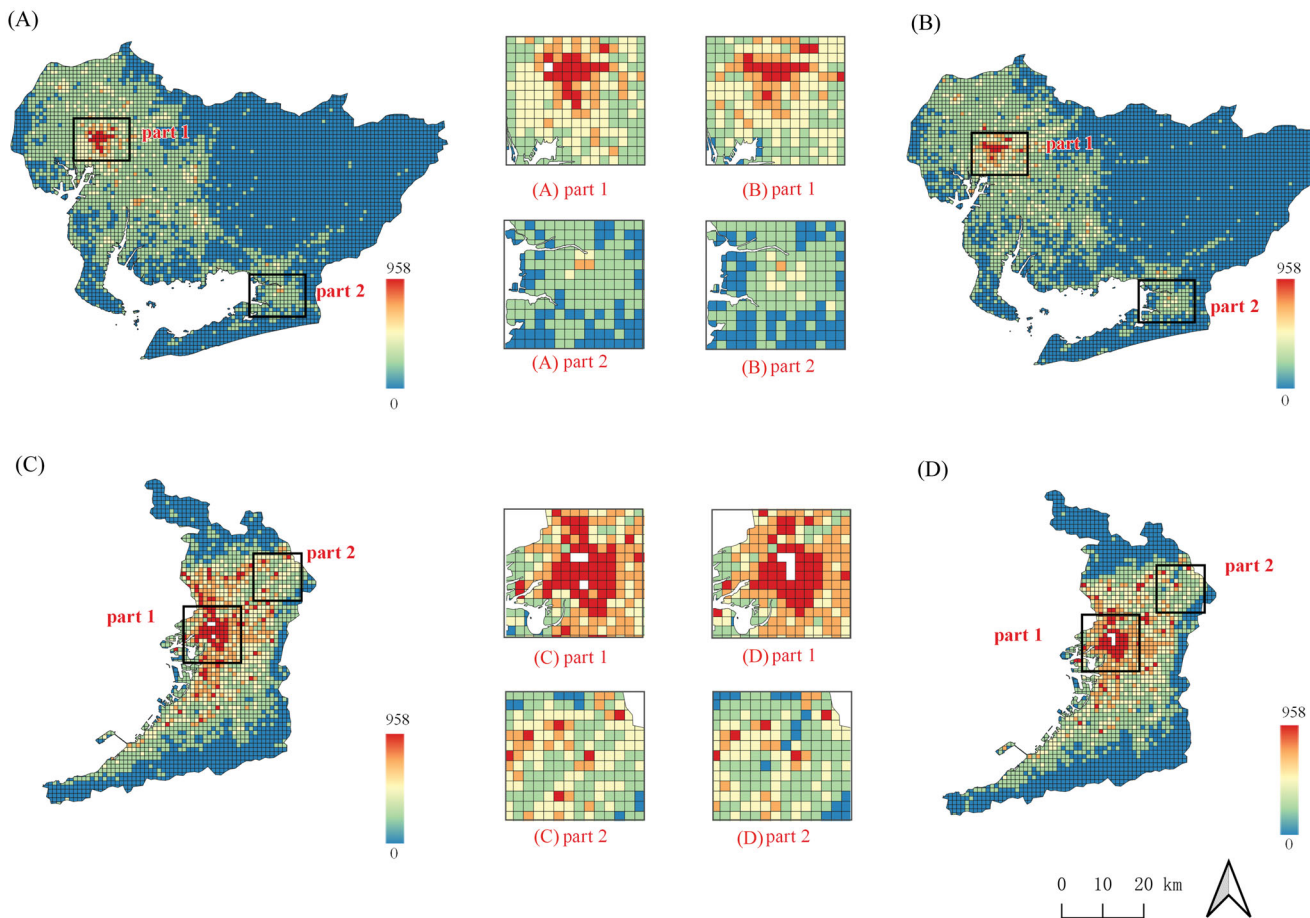


**Figure 12.** Heat maps of demographic density without warning and after disaster warning. Aichi Prefecture and Osaka City were selected for in-depth study. (A) and (C) are heat maps in Aichi Prefecture and Osaka City at 12:00 a.m. on 5/26. (B) and (D) are heat maps in Aichi Prefecture and Osaka City at 12:00 a.m. on 6/2, respectively.

protect themselves in an emergency. Meanwhile, cross-sectoral collaboration between government agencies, the private sector, nongovernmental organizations, and community-based organizations should be strengthened to help ensure that disaster response plans are comprehensive and coordinated.

In addition, we found that early warning data can influence human mobility behavior in the face of extreme rainfall events. We collected data on early warning systems regarding the issuance of rainstorm, flood, and fog warnings in the study area at 10:52 a.m. on 6/2. Subsequently, using large-scale individual trajectory data, we conducted a statistical analysis and mapped the demographic heat distribution in the study area, comparing the

situation on Friday, 26 May 2023 (hereinafter 5/26), with Friday, 6/2, at 12:00 a.m. The results, depicted in Figure 12, indicate a 14 percent (Table 3) average reduction in population activity following the warnings. This suggests that rainstorms and flood warnings can influence human travel behavior, although the extent of the change is not particularly large. This exploration can assist decision makers in optimizing the design and implementation of early warning systems for disaster preparedness and response strategies.

The study area's topography features higher elevations in the northeast and south, with plains and hills dominating the landscape. The central region is flatter and crossed by several rivers, and the

**Table 3.** Magnitude of change in population movements without warning and after disaster warning

	Flash flood warning (1 hour after warning)	Without warning (same moment)	Magnitude of change (percent)
Population heat value	156,218	178,088	-14.00

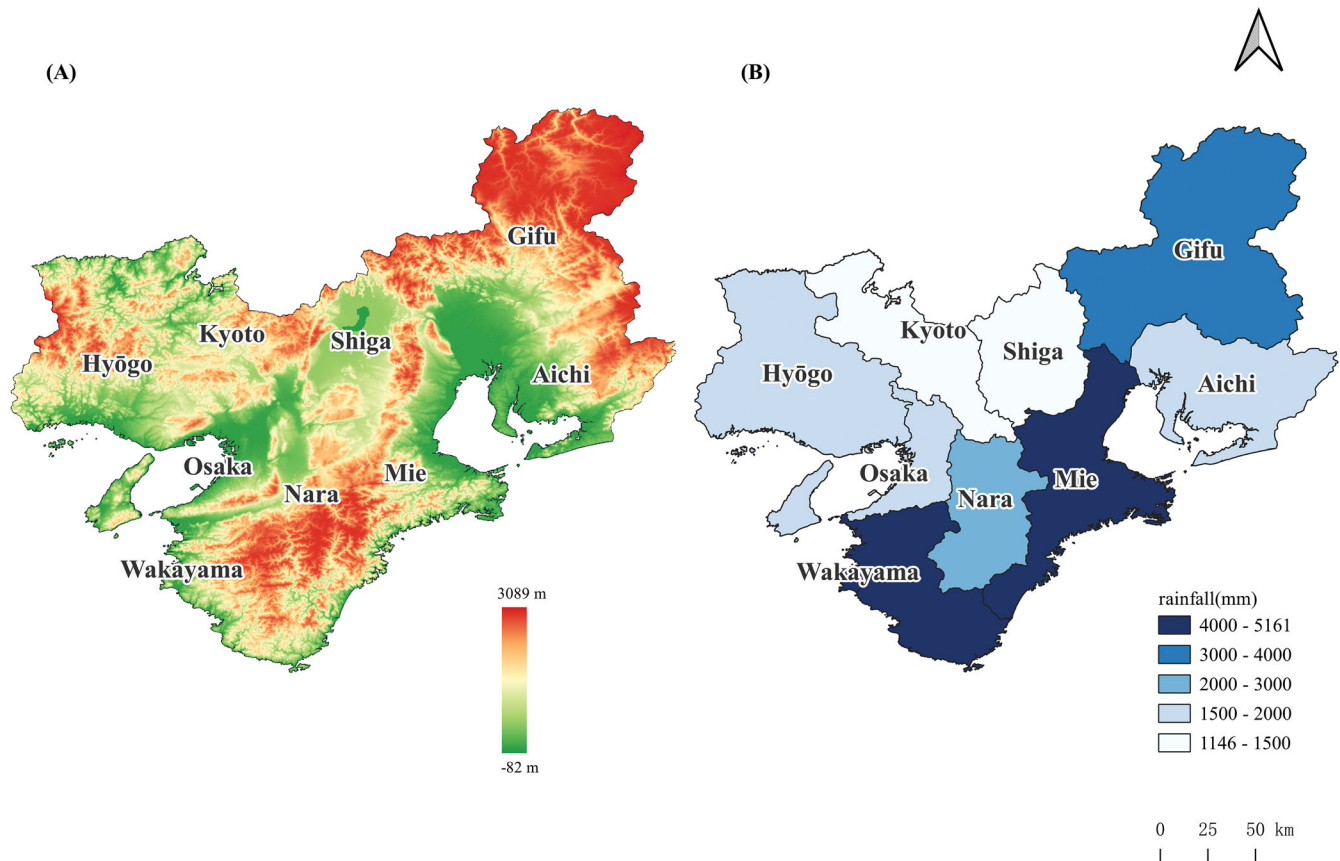


**Figure 13.** (A) Digital Elevation Model elevation map of the study area. (B) Rainfall distribution on 6/2 during the simulated rainstorm event.



southeastern region borders the coastline. The diverse topographies influence rainfall distribution. The varying relief significantly affects atmospheric dynamics, affecting air movement patterns and moisture ascent, thereby affecting cloud formation and precipitation processes. Analysis of the DEM topographic map and rainfall distribution map, achieved through hierarchical rendering and visual comparison of the two maps, reveals higher rainfall in the elevated hilly areas and southeastern coastal regions due to monsoon influence in June. These findings align with intuitive expectations (Figure 13).

The diverse topography of the study area affects human mobility patterns. Our examination of the distribution of human mobility resilience patterns, depicted in the DEM topographic map and Figure 8, indicates minimal human activity in the higher terrain and hilly areas. It is important to note, however, that during heavy rainfall and flooding events, the undulations and slopes of the terrain play a crucial role in directing and slowing water flow, consequently affecting inundation levels and evacuation routes. Low-lying areas are prone to waterlogging, leading to disruption of transportation and stranding of residents. Conversely, elevated regions can serve as temporary refuges due to their reduced susceptibility to flooding. Furthermore, the terrain influences the access routes for rescue teams and the distribution of rescue supplies. Future studies can take topographical factors into account when planning the site for emergency resource allocation points and places of refuge.

### Limitation

Although data-driven and complex systems-based approaches are important for studying resilience, it is crucial to acknowledge the limitations of trajectory data, which are often derived from cell phones or Global Positioning System (GPS) devices. Only a portion of the entire population with selected demographic labels is covered, and there might also be issues of imbalance and representativeness. Furthermore, these data can only cover the people who use these devices and do not give a complete picture of everyone's mobility. Future research could benefit from incorporating multisource trajectory data to provide a more comprehensive understanding of overall mobility patterns.

### Conclusion

In coping with the complexity of urban systems, large-scale trajectory data and resilience curves have been used as a vital methodology to study urban resilience during extreme disasters. We propose a framework for studying multiscale human mobility resilience patterns under extremely hazardous conditions, aiming at the problem of fewer studies on multiscale resilience patterns and the lack of investigation on the distribution pattern and causes of resilience anomalies. We construct a dynamic network based on large-scale trajectory data to analyze human mobility during rainfall events. We also evaluate urban resilience by resilience curve definition and quantify resilience patterns using quadrant plots. Furthermore, we explore the relationship between urban RLs, resilience patterns, and social factors. Our findings disclose that extreme disasters reduce human mobility level but do not radically reduce connectivity with many peripheral areas in the network. Additionally, we find numerous abnormal resilience patterns in human mobility, which are closely related to the local geographical settings of the built environment. Populations with different demographic and socioeconomic characteristics behave differently. This study provides valuable insights into the vulnerability and risks faced by the built environment. It equips decision makers with crucial information to enhance postdisaster recovery efforts and inform urban infrastructure planning. By aiding cities in adapting to shifting climatic conditions, the study mitigates the adverse impact of extreme weather events on the safety and well-being of urban residents and their property. Our findings can serve as a reference for emergency management decisions and long-term urban agglomeration planning and preparedness.

Future studies can focus on enhancing urban resilience and human mobility recovery during extreme storm events through improved urban planning and disaster risk management. Given the influence of early warning data on human mobility found in this study, examining the impact of various rainstorm warning strategies on human mobility resilience is crucial. This analysis will help decision makers optimize the design and implementation of early warning systems, thereby improving disaster preparedness and response. In addition, assessing and optimizing the



spatial distribution of emergency resource points could ensure that support reaches affected areas swiftly and efficiently during disasters. Overall, enhancing early warning systems, improving resource allocation, and refining urban planning and disaster management practices are essential for cities to effectively manage and withstand extreme weather events.

## Disclosure Statement


No potential conflict of interest was reported by the authors.

## Funding

This work was supported by the National Natural Science Foundation of China (42471491, 42171466), the National Key Research and Development Program of China (2023YFB3906803), the Key Laboratory of Earth Surface System and Human-Earth Relations, Ministry of Natural Resources of China (LBXT2023YB03), and the “CUG Scholar” Scientific Research Funds at China University of Geosciences (Wuhan; 2022034). This work was partly supported by the Project Grant from the Co-creation Center for Disaster Resilience, IRIDeS, Tohoku University (ID: 2-QR001). The research was partially conducted at the Future Resilient Systems program at the Singapore-ETH Centre, supported by the National Research Foundation (NRF) Singapore under its Campus for Research Excellence and Technological Enterprise (CREATE) program.

## ORCID

Yao Yao  <http://orcid.org/0000-0002-2830-0377>

Yatao Zhang  <http://orcid.org/0000-0001-5701-2836>

Qingfeng Guan  <http://orcid.org/0000-0002-7392-3709>

## References

Barrett, C. B., K. Ghezzi-Kopel, J. Hoddinott, N. Homami, E. Tennant, J. Upton, and T. Wu. 2021. A scoping review of the development resilience

literature: Theory, methods and evidence. *World Development* 146:105612. doi: [10.1016/j.worlddev.2021.105612](https://doi.org/10.1016/j.worlddev.2021.105612).

- Batty, M. 2013. Big data, smart cities and city planning. *Dialogues in Human Geography* 3 (3):274–79. doi: [10.1177/2043820613513390](https://doi.org/10.1177/2043820613513390).
- Cimellaro, G. P., A. M. Reinhorn, and M. Bruneau. 2010. Framework for analytical quantification of disaster resilience. *Engineering Structures* 32 (11):3639–49. doi: [10.1016/j.engstruct.2010.08.008](https://doi.org/10.1016/j.engstruct.2010.08.008).
- Cutter, S. L., L. Barnes, M. Berry, C. Burton, E. Evans, E. Tate, and J. Webb. 2008. A place-based model for understanding community resilience to natural disasters. *Global Environmental Change* 18 (4):598–606. doi: [10.1016/j.gloenvcha.2008.07.013](https://doi.org/10.1016/j.gloenvcha.2008.07.013).
- Duan, X., T. Zhang, Z. Xu, Q. Wan, J. Yan, W. Wang, and Y. Tian. 2023. Discovering urban mobility structure: A spatio-temporal representational learning approach. *International Journal of Digital Earth* 16 (2):4044–72. doi: [10.1080/17538947.2023.2261769](https://doi.org/10.1080/17538947.2023.2261769).
- Fang, C. L., Z. B. Wang, and H. T. Ma. 2018. The theoretical cognition of the development law of China's urban agglomeration and academic contribution. *Acta Geographica Sinica* 73 (4):651–65. doi: [10.11821/dlxb201804005](https://doi.org/10.11821/dlxb201804005).
- Gong, L., M. Jin, Q. Liu, Y. Gong, and Y. Liu. 2020. Identifying urban residents' activity space at multiple geographic scales using mobile phone data. *ISPRS International Journal of Geo-Information* 9 (4):241. doi: [10.3390/ijgi9040241](https://doi.org/10.3390/ijgi9040241).
- Guo, K., X. Huang, L. Wu, and Y. Chen. 2022. Local community detection algorithm based on local modularity density. *Applied Intelligence* 52 (2):1238–53. doi: [10.1007/s10489-020-02052-0](https://doi.org/10.1007/s10489-020-02052-0).
- Hallegatte, S., A. Vogt-Schilb, M. Bangalore, and J. Rozenberg. 2016. *Unbreakable: Building the resilience of the poor in the face of natural disasters*. Washington, DC: World Bank Publications.
- Haraguchi, M., A. Nishino, A. Kodaka, M. Allaire, U. Lall, L. Kuei-Hsien, K. Onda, K. Tsubouchi, and N. Kohtake. 2022. Human mobility data and analysis for urban resilience: A systematic review. *Environment and Planning B: Urban Analytics and City Science* 49 (5):1507–35. doi: [10.1177/23998083221075634](https://doi.org/10.1177/23998083221075634).
- Hino, M., and E. Nance. 2021. Five ways to ensure flood-risk research helps the most vulnerable. *Nature* 595 (7865):27–29. doi: [10.1038/d41586-021-01750-0](https://doi.org/10.1038/d41586-021-01750-0).
- Holling, C. S. 1973. Resilience and stability of ecological systems. *Annual Review of Ecology and Systematics* 4 (1):1–23. doi: [10.1146/annurev.es.04.110173.000245](https://doi.org/10.1146/annurev.es.04.110173.000245).
- Hong, B., B. J. Bonczak, A. Gupta, and C. E. Kontokosta. 2021. Measuring inequality in community resilience to natural disasters using large-scale mobility data. *Nature Communications* 12 (1):1870. doi: [10.1038/s41467-021-22160-w](https://doi.org/10.1038/s41467-021-22160-w).
- Hossain, E., S. Roy, N. Mohammad, N. Nawar, and D. R. Dipta. 2021. Metrics and enhancement strategies for grid resilience and reliability during natural disasters. *Applied Energy* 290:116709. doi: [10.1016/j.apenergy.2021.116709](https://doi.org/10.1016/j.apenergy.2021.116709).

- Jia, X., B. Hu, B. P. Marchant, L. Zhou, Z. Shi, and Y. Zhu. 2019. A methodological framework for identifying potential sources of soil heavy metal pollution based on machine learning: A case study in the Yangtze Delta, China. *Environmental Pollution* 250:601–09. doi: [10.1016/j.envpol.2019.04.047](https://doi.org/10.1016/j.envpol.2019.04.047).
- Kontokosta, C. E., and A. Malik. 2018. The Resilience to Emergencies and Disasters Index: Applying big data to benchmark and validate neighborhood resilience capacity. *Sustainable Cities and Society* 36:272–85. doi: [10.1016/j.scs.2017.10.025](https://doi.org/10.1016/j.scs.2017.10.025).
- Kraemer, M. U. G., A. Sadilek, Q. Zhang, N. A. Marchal, G. Tuli, E. L. Cohn, Y. Hswen, T. A. Perkins, D. L. Smith, R. C. Reiner, Jr., et al. 2020. Mapping global variation in human mobility. *Nature Human Behaviour* 4 (8):800–10. doi: [10.1038/s41562-020-0875-0](https://doi.org/10.1038/s41562-020-0875-0).
- Kryvasheyev, Y., H. Chen, N. Obradovich, E. Moro, P. Van Hentenryck, J. Fowler, and M. Cebrian. 2016. Rapid assessment of disaster damage using social media activity. *Science Advances* 2 (3):e1500779. doi: [10.1126/sciadv.1500779](https://doi.org/10.1126/sciadv.1500779).
- Li, Z. Z., D. F. Fu, J. X. Wang, and K. D. Min. 2022. Urban resilience assessment model for waterlogging disasters and its application. *Journal of Tsinghua University (Science and Technology)* 62 (2):266–76. doi: [10.16511/j.cnki.qhdxxb.2021.22.037](https://doi.org/10.16511/j.cnki.qhdxxb.2021.22.037).
- Liao, K. 2012. A theory on urban resilience to floods—A basis for alternative planning practices. *Ecology and Society* 17 (4):48. doi: [10.5751/ES-05231-170448](https://doi.org/10.5751/ES-05231-170448).
- Linkov, I., S. Carluccio, O. Pritchard, A. Ni Bhreasail, S. Galaitsi, J. Sarkis, and J. M. Keisler. 2020. The case for value chain resilience. *Management Research Review* 43 (12):1461–76. doi: [10.1108/MRR-08-2019-0353](https://doi.org/10.1108/MRR-08-2019-0353).
- Meerow, S., J. P. Newell, and M. Stults. 2016. Defining urban resilience: A review. *Landscape and Urban Planning* 147:38–49. doi: [10.1016/j.landurbplan.2015.11.011](https://doi.org/10.1016/j.landurbplan.2015.11.011).
- Mehrabi, Z., R. Delzeit, A. Ignaciuk, C. Levers, G. Braich, K. Bajaj, A. Amo-Aidoo, W. Anderson, R. A. Balgah, T. G. Benton, et al. 2022. Research priorities for global food security under extreme events. *One Earth* 5 (7):756–66. doi: [10.1016/j.oneear.2022.06.008](https://doi.org/10.1016/j.oneear.2022.06.008).
- Panteli, M., P. Mancarella, D. N. Trakas, E. Kyriakides, and N. D. Hatziaargyriou. 2017. Metrics and quantification of operational and infrastructure resilience in power systems. *IEEE Transactions on Power Systems* 32 (6):4732–42. doi: [10.1109/TPWRS.2017.2664141](https://doi.org/10.1109/TPWRS.2017.2664141).
- Perera, A., and T. Hong. 2023. Vulnerability and resilience of urban energy ecosystems to extreme climate events: A systematic review and perspectives. *Renewable and Sustainable Energy Reviews* 173:113038. doi: [10.1016/j.rser.2022.113038](https://doi.org/10.1016/j.rser.2022.113038).
- Petraroli, I., and R. Baars. 2022. To be a woman in Japan: Disaster vulnerabilities and gendered discourses in disaster preparedness in Japan. *International Journal of Disaster Risk Reduction* 70:102767. doi: [10.1016/j.ijdrr.2021.102767](https://doi.org/10.1016/j.ijdrr.2021.102767).
- Pimm, S. L., I. Donohue, J. M. Montoya, and M. Loreau. 2019. Measuring resilience is essential to understand it. *Nature Sustainability* 2 (10):895–97. doi: [10.1038/s41893-019-0399-7](https://doi.org/10.1038/s41893-019-0399-7).
- Poulin, C., and M. B. Kane. 2021. Infrastructure resilience curves: Performance measures and summary metrics. *Reliability Engineering & System Safety* 216:107926. doi: [10.1016/j.res.2021.107926](https://doi.org/10.1016/j.res.2021.107926).
- Reichstein, M., F. Riede, and D. Frank. 2021. More floods, fires and cyclones—Plan for domino effects on sustainability goals. *Nature* 592 (7854):347–49. doi: [10.1038/d41586-021-00927-x](https://doi.org/10.1038/d41586-021-00927-x).
- Rentschler, J., M. Salhab, and B. A. Jafino. 2022. Flood exposure and poverty in 188 countries. *Nature Communications* 13 (1):3527. doi: [10.1038/s41467-022-30727-4](https://doi.org/10.1038/s41467-022-30727-4).
- Ronco, M., J. M. Tárraga, J. Muñoz, M. Piles, E. S. Marco, Q. Wang, M. T. M. Espinosa, S. Ponserré, and G. Camps-Valls. 2023. Exploring interactions between socioeconomic context and natural hazards on human population displacement. *Nature Communications* 14 (1):8004. doi: [10.1038/s41467-023-43809-8](https://doi.org/10.1038/s41467-023-43809-8).
- Rus, K., V. Kilar, and D. Koren. 2018. Resilience assessment of complex urban systems to natural disasters: A new literature review. *International Journal of Disaster Risk Reduction* 31:311–30. doi: [10.1016/j.ijdrr.2018.05.015](https://doi.org/10.1016/j.ijdrr.2018.05.015).
- Santana, C., F. Botta, H. Barbosa, F. Privitera, R. Menezes, and R. Di Clemente. 2023. COVID-19 is linked to changes in the time–space dimension of human mobility. *Nature Human Behaviour* 7 (10):1729–39. doi: [10.1038/s41562-023-01660-3](https://doi.org/10.1038/s41562-023-01660-3).
- Sarker, M. N. I., Y. Peng, C. Yiran, and R. C. Shouse. 2020. Disaster resilience through big data: Way to environmental sustainability. *International Journal of Disaster Risk Reduction* 51:101769. doi: [10.1016/j.ijdrr.2020.101769](https://doi.org/10.1016/j.ijdrr.2020.101769).
- Scott, D., C. M. Hall, B. Rushton, and S. Gössling. 2024. A review of the IPCC Sixth Assessment and implications for tourism development and sectoral climate action. *Journal of Sustainable Tourism* 32 (9):1725–42. doi: [10.1080/09669582.2023.2195597](https://doi.org/10.1080/09669582.2023.2195597).
- Sharifi, A., and Y. Yamagata. 2016. Principles and criteria for assessing urban energy resilience: A literature review. *Renewable and Sustainable Energy Reviews* 60:1654–77. doi: [10.1016/j.rser.2016.03.028](https://doi.org/10.1016/j.rser.2016.03.028).
- Shi, H., P. Wang, J. Zheng, Y. Deng, C. Zhuang, F. Huang, and R. Xiao. 2023. A comprehensive framework for identifying contributing factors of soil trace metal pollution using Geodetector and spatial bivariate analysis. *The Science of the Total Environment* 857 (Pt. 3):159636. doi: [10.1016/j.scitotenv.2022.159636](https://doi.org/10.1016/j.scitotenv.2022.159636).
- Smiley, K. T., I. Noy, M. F. Wehner, D. Frame, C. C. Sampson, and O. E. Wing. 2022. Social inequalities in climate change-attributed impacts of Hurricane Harvey. *Nature Communications* 13 (1):3418. doi: [10.1038/s41467-022-31056-2](https://doi.org/10.1038/s41467-022-31056-2).
- Tang, J., P. Zhao, Z. Gong, H. Zhao, F. Huang, J. Li, Z. Chen, L. Yu, and J. Chen. 2023. Resilience patterns of human mobility in response to extreme urban floods. *National Science Review* 10 (8):nwad097. doi: [10.1093/nsr/nwad097](https://doi.org/10.1093/nsr/nwad097).

- Tong, P. 2021. Characteristics, dimensions and methods of current assessment for urban resilience to climate-related disasters: A systematic review of the literature. *International Journal of Disaster Risk Reduction* 60:102276. doi: [10.1016/j.ijdr.2021.102276](https://doi.org/10.1016/j.ijdr.2021.102276).
- United Nations. 2018. *Revision of world urbanization prospects*. New York: United Nations.
- Yao, Y., Z. Guo, X. Huang, S. Ren, Y. Hu, A. Dong, and Q. Guan. 2023. Gauging urban resilience in the United States during the COVID-19 pandemic via social network analysis. *Cities* 138:104361. doi: [10.1016/j.cities.2023.104361](https://doi.org/10.1016/j.cities.2023.104361).
- Yao, Y., X. Li, X. Liu, P. Liu, Z. Liang, J. Zhang, and K. Mai. 2017. Sensing spatial distribution of urban land use by integrating points-of-interest and Google Word2Vec model. *International Journal of Geographical Information Science* 31 (4):825–48. doi: [10.1080/13658816.2016.1244608](https://doi.org/10.1080/13658816.2016.1244608).
- Yu, M., S. Zhang, H. Ning, Z. Li, and K. Zhang. 2024. Assessing the 2023 Canadian wildfire smoke impact in Northeastern US: Air quality, exposure and environmental justice. *The Science of the Total Environment* 926:171853. doi: [10.1016/j.scitotenv.2024.171853](https://doi.org/10.1016/j.scitotenv.2024.171853).
- Yuan, J., K. Chen, W. Li, C. Ji, Z. Wang, and M. J. Skibniewski. 2018. Social network analysis for social risks of construction projects in high-density urban areas in China. *Journal of Cleaner Production* 198:940–61. doi: [10.1016/j.jclepro.2018.07.109](https://doi.org/10.1016/j.jclepro.2018.07.109).
- Zhang, F., Z. Li, N. Li, and D. Fang. 2019. Assessment of urban human mobility perturbation under extreme weather events: A case study in Nanjing, China. *Sustainable Cities and Society* 50:101671. doi: [10.1016/j.scs.2019.101671](https://doi.org/10.1016/j.scs.2019.101671).
- Zhang, X., and N. Li. 2022. Characterizing individual mobility perturbations in cities during extreme weather events. *International Journal of Disaster Risk Reduction* 72:102849. doi: [10.1016/j.ijdr.2022.102849](https://doi.org/10.1016/j.ijdr.2022.102849).
- Zhang, Y., S. Song, X. Li, S. Gao, and M. Raubal. 2024. Leveraging context-adjusted nighttime light data for socioeconomic explanations of global urban resilience. *Sustainable Cities and Society* 114:105739. doi: [10.1016/j.scs.2024.105739](https://doi.org/10.1016/j.scs.2024.105739).

YAO YAO is a Professor at China University of Geosciences, Wuhan, China, 430078, and a Researcher at the Center for Spatial Information Science at the University of Tokyo, Tokyo, Japan. E-mail: [yaoy@cug.edu.cn](mailto:yaoy@cug.edu.cn). His research interests include geospatial big data mining, analysis, and urban computing.

LIN LIANG is a Graduate Student at China University of Geosciences, Wuhan, China, 430078. E-mail: [lianglin@cug.edu.cn](mailto:lianglin@cug.edu.cn). Her research interests include spatiotemporal big data mining and urban planning.

YATAO ZHANG is a Doctoral Candidate at the Future Resilient Systems Program, Singapore-ETH Center, ETH Zurich, Singapore 138602. E-mail: [yatzhang@ethz.ch](mailto:yatzhang@ethz.ch). His research interests lie in GeoAI, context-based spatiotemporal analysis, and urban computing.

YUJIA WANG is a Graduate Student at China University of Geosciences, Wuhan, China, 430078. E-mail: [WangYujia@cug.edu.cn](mailto:WangYujia@cug.edu.cn). Her research interests include spatiotemporal big data mining, spatial optimization, and spatial equity.

ZHIHUI HU is a Graduate Student at China University of Geosciences, Wuhan, China, 430078. E-mail: [zihui.hu@cug.edu.cn](mailto:zihui.hu@cug.edu.cn). His research interests include geospatial big data mining and land-use classification.

YUNPENG FAN is a Graduate Student at China University of Geosciences, Wuhan, China, 430078. E-mail: [fanyunpeng@cug.edu.cn](mailto:fanyunpeng@cug.edu.cn). His research interests include urban logistics optimization and deep reinforcement learning.

QINGFENG GUAN is a Professor at China University of Geosciences, Wuhan, China, 430078. E-mail: [guanqf@cug.edu.cn](mailto:guanqf@cug.edu.cn). His research interests include high-performance spatial intelligence computation and urban computing.

RENHE JIANG is an Associate Professor at the Center for Spatial Information Science at the University of Tokyo, Tokyo, Japan. E-mail: [jiangrh@csis.u-tokyo.ac.jp](mailto:jiangrh@csis.u-tokyo.ac.jp). His research interests include ubiquitous computing, deep learning, and spatiotemporal data analysis.

RYOSUKE SHIBASAKI is a Project Professor at the School of Interdisciplinary Information Studies at the University of Tokyo, Tokyo, Japan. E-mail: [shiba@csis.u-tokyo.ac.jp](mailto:shiba@csis.u-tokyo.ac.jp). His research interests cover mobile big data analysis, satellite and aerial imagery, and sensor data analysis, including automated mapping with deep learning, human behavior modeling and simulation, and data assimilation of discrete moving objects.